Integration of Two In-depth Quantitative Proteomics Approaches Determines the Kallikrein-related Peptidase 7 (KLK7) Degradome in Ovarian Cancer Cell Secretome

Authors

Lakmali Munasinghage Silva, Thomas Kryza, Thomas Stoll, Christine Hoogland, Ying Dong, Carson Ryan Stephens, Marcus Lachlan Hastie, Viktor Magdolen, Oded Kleifeld, Jeffrey John Gorman, and Judith Ann Clements

Correspondence

munasinghage.silva@nih.gov;
j.clements@qut.edu.au

In Brief

KLK7 secreted by ovarian cancer cells into the peritoneal fluid may aid in cancer progression. To evaluate the functional role of KLK7 in this context, knowledge on its substrate repertoire is crucial. Herein, using two proteomics approaches, qPROTOMAP and TAILS, we identified pro-MMP10, thrombospondin 1 and IGFBP6 as putative KLK7 substrates in an *in vitro* setting.

Graphical Abstract

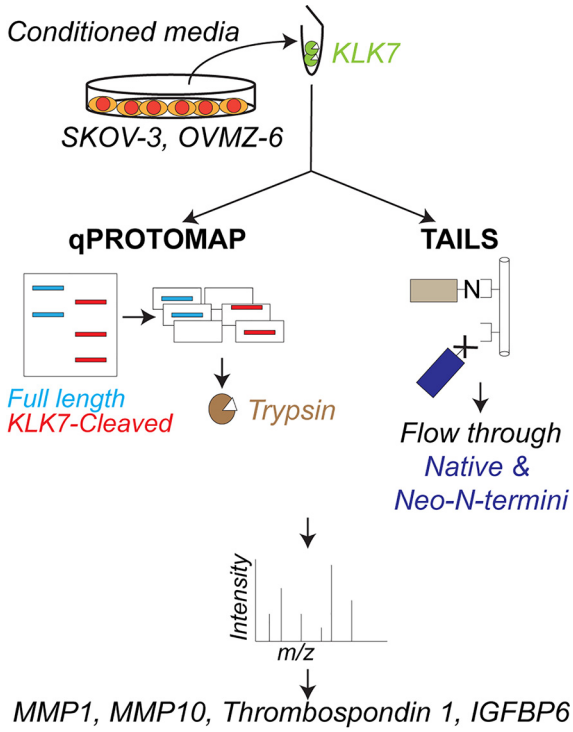

Highlights

- Kallikrein-related peptidase 7 is over expressed in ovarian cancer.
- Quantitative PROTOMAP and TAILS approaches identified putative substrates of KLK7.
- Pro-MMP10 is activated by KLK7.
- KLK7 cleaves thrombospondin 1 and IGFBP6 *in vitro*.

Silva et al., 2019, Molecular & Cellular Proteomics *18*, 818–836

https://doi.org/10.1074/mcp.RA118.001304

Integration of Two In-depth Quantitative Proteomics Approaches Determines the Kallikrein-related Peptidase 7 (KLK7) Degradome in Ovarian Cancer Cell Secretome*[S]

Lakmali Munasinghage Silva‡**‡‡, Thomas Kryza‡**, Thomas Stoll§, Christine Hoogland§**, Ying Dong‡, Carson Ryan Stephens‡**, Marcus Lachlan Hastie§, Viktor Magdolen‖, Oded Kleifeld¶**, Jeffrey John Gorman§, and Judith Ann Clements‡§§

Kallikrein-related peptidase 7 (KLK7) is a serine peptidase that is over expressed in ovarian cancer. *In vitro* functional analyses have suggested KLK7 to play a cancer progressive role, although monitoring of KLK7 expression has suggested a contradictory protective role for KLK7 in ovarian cancer patients. In order to help delineate its mechanism of action and thereby the functional roles, information on its substrate repertoire is crucial. Therefore, in this study a quantitative proteomics approach—PROtein TOpography and Migration Analysis Platform (PROTOMAP)—coupled with SILAC was used for in-depth analysis of putative KLK7 substrates from a representative ovarian cancer cell line, SKOV-3, secreted proteins. The Terminal Amine Isotopic Labeling of Substrates (TAILS) approach was used to determine the exact cleavage sites and to validate qPROTOMAP-identified putative substrates. By employing these two technically divergent approaches, exact cleavage sites on 16 novel putative substrates and two established substrates, matrix metalloprotease (MMP) 2 and insulin growth factor binding protein 3 (IGFBP3), were identified in the SKOV-3 secretome. Eight of these substrates were also identified on TAILS analysis of another ovarian cancer cell (OVMZ-6) secretome, with a further seven OVMZ-6 substrates common to the SKOV-3 qPROTOMAP profile. Identified substrates were significantly associated with the common processes of cell adhesion, extracellular matrix remodeling and cell migration according to the gene ontology (GO) biological process analysis. Biochemical validation supports a role for KLK7 in directly activating pro-MMP10, hydrolysis of IGFBP6 and cleavage of thrombospondin 1 with generation of a potentially bioactive N-terminal fragment. Overall, this study constitutes the most comprehensive analysis of the putative KLK7 degradome in any cancer to date, thereby opening new avenues for KLK7 research. *Molecular & Cellular Proteomics 18: 818–836, 2019. DOI: 10.1074/mcp.RA118.001304.*

Kallikrein-related peptidase (KLK[1]) 7 is a secreted serine peptidase that is over expressed in pathological conditions, including ovarian cancer. Ovarian cancer is the leading cause of death from gynecological malignancies despite its relatively low level of occurrence (1). Ascites plays a major role in ovarian cancer progression by accumulating shed malignant cells as aggregates, promoting cell survival and leading to peritoneal dissemination (2–5). These cells floating within the ascites harbor a metastatic preference and secrete factors, such as peptidases, that either facilitate disease progression or inhibition by modulating the surrounding microenvironment. KLK7 is secreted by the cells that are present in the ascites (6).

Functional studies performed to date have suggested KLK7 has cancer progressive properties (4), although, in clinical studies the increased expression of KLK7 has been shown to be associated with a protective impact on overall survival of ovarian cancer patients (7, 8). Knowledge of the putative KLK7 substrate repertoire secreted by cancer cells in the

From the ‡Queensland University of Technology (QUT), Institute of Health and Biomedical Innovation (IHBI) and School of Biomedical Sciences at the Translational Research Institute, 37 Kent Street, Woolloongabba, Queensland, 4102, Australia; §Protein Discovery Centre, QIMR Berghofer Medical Research Institute, 300 Herston Road, Herston, Queensland, 4006, Australia; ¶Department of Biochemistry and Molecular Biology, School of Biomedical Sciences, Monash University, Victoria, Australia 3800; ‖Klinische Forschergruppe der Frauenklinik, Klinikum Rechts der Isar, TU München, Munich, Germany

Received December 31, 2018
Published, MCP Papers in Press, January 31, 2019, DOI 10.1074/mcp.RA118.001304

ascites microenvironment is thus fundamental to determine the functional role of KLK7 in cancer.

To date, KLK7 substrates have been identified, a priori, in a biochemical context by incubating recombinant proteins with the KLK7 peptidase *in vitro*, with minimal representation of cellular context and physiological conditions. No studies to date have assessed KLK7-mediated proteolysis in ovarian cancer cells using in-depth proteomics approaches (9). To this end, we sought to use two proteomic profiling approaches namely PROtein TOpography and Migration Analysis Platform (PROTOMAP) (10) and Terminal Amine Isotopic Labeling of Substrates (TAILS) (11) to identify putative KLK7 substrates and their exact cleavage sites in ovarian cancer using the secretome of representative ovarian cancer cells. This study thereby identified 23 putative novel KLK7 substrates increasing the number of currently identified putative KLK7 substrates, thus providing an excellent base for future research into the functional role of KLK7 in ovarian cancer.

EXPERIMENTAL PROCEDURES

Cell Lines and Cell Culture—The SKOV-3 (the American Type Culture Collection, ATCC[1]) cell line, derived from a patient with moderately well differentiated adenocarcinoma (12, 13), was maintained (37 °C, 5% (v/v) CO_2) in phenol red-free RPMI 1640 media with 2 mM L-glutamine (Life Technologies, VIC, Australia) supplemented with 10% (v/v) fetal bovine serum (FBS; Sigma-Aldrich, Carlsbad, CA). The OVMZ-6 cell line derived from a FIGO Stage IV poorly differentiated serous adenocarcinoma (14) was maintained in DMEM with high glucose, Glutamax-I and pyridoxine (Invitrogen, Life Technologies), with 10% FBS, 10 mM HEPES, 0.55 mM L-arginine, 0.272 mM L-asparagine and 20 μg/ml gentamycin. All cell lines were regularly screened for mycoplasma contamination.

Conditioned Media Collection—SKOV-3 and OVMZ-6 cells were grown to 70% confluence, depleted of serum proteins and after 24 h conditioned media (CM) was collected. Cleared CM in the presence of 50 μM EDTA was concentrated and buffer-exchanged into assay buffer (1× PBS pH 8.0, Amicon Ultra-15 centrifugal filter units). The protein concentration was measured using the BCA method (Sigma Aldrich) and adjusted to 1 mg/ml using assay buffer.

Production of Recombinant KLK7 and dmKLK7—Recombinant active KLK7 and a catalytically inactive double mutant KLK7 (dmKLK7) were produced and purified in the *Pichia pastoris* expression system and the percent active material in the produced KLK7 sample was measured using active site titration against human (rh) Serpin A3/α1-Antichymotrypsin as described elsewhere (15). Throughout the study KLK7 concentration was calculated considering the percent active material as determined by active site titration.

Experimental Design and Statistical Rationale—Three independent biological replicates were used for each proteomics analysis. Criteria for protein identification: for qPROTOMAP analysis MaxQuant (version 1.5.0.30) was used. For TAILS analysis, X!Tandem (release 2009.10.01.1 LabKey, Insilicos, Institute for Systems Biology) contained within the TPP (v4.6) was used. Quantitation was based on unique peptides only and a minimum of two ratio counts was required. In both approaches peptide identifications were accepted if they could be established at a FDR ≤1%. Data from each of three biological replicates from two proteomics approaches was analyzed independent of other replicates and proteomics approaches. MS data have been deposited to the ProteomeXchange consortium (http://proteomecentral.proteomexchange.org) via the PRIDE partner repository (16). Zipped MaxQuant ".txt" files including ".wiff" files have been deposited with the dataset identifier PXD003812 for SKOV-3 qPROTOMAP analysis. The TAILS MS files have been deposited with the dataset identifier PXD003752 or DOI: 10.6019/PXD003752 for SKOV-3 and PXD004591 or DOI: 10.6019/PXD004591 for OVMZ-6.

Screening for KLK7 Substrates in SKOV-3 Cell Secretome Using qPROTOMAP—

Stable Isotope Labeling by Amino acids in Cell culture (SILAC) Media Preparation and Cell Culture—For SKOV-3 labeling, RPMI 1640 media (deficient in L-Lysine, and L-Arginine; Sigma-Aldrich) was prepared by adding either L-Lysine (40.00 mg/L, Sigma-Aldrich) and L-arginine (50.0825 mg/L, Sigma-Aldrich) or L-D_4-Lysine (K4, 40.8632 mg/L, Sigma-Aldrich) and L-Arginine.HCl [U-$^{13}C_6$, 99%] (R6, 62.2466 mg/L, Cambridge Isotope Laboratories, Tewksbury, MA) or L-Lysine.2HCl [U-$^{13}C_6$, 99%; U-$^{15}N_2$, 99%] (K8, 41.7063 mg/L, Cambridge Isotope Laboratories) and L-Arginine.HCl [U-$^{13}C_6$, 99%; U-$^{15}N_4$, 99%] (R10, 63.365 mg/L, Cambridge Isotope Laboratories) to make Light, Medium or Heavy labeling media, respectively. Cells were passaged as in section Cell Lines and Cell Culture with 10% dialyzed FBS (Invitrogen, US Origin) and at passage 6 cell lysates were MS analyzed to determine >95% of SILAC incorporation. Note: a quarter (0.2875 mM) of the arginine present in commercial RPMI 1640 media (1.1494 mM) was used for SILAC labeling in order to prevent arginine to proline conversion under extra arginine concentrations (17).

Treating SILAC-SKOV-3 Cell Conditioned Media with KLK7 and dmKLK7—Light, medium and heavy CM (20 μg each) was treated with KLK7 (1:50; active site-titrated KLK7:CM; *w/w*) or equivalent amounts of dmKLK7 or assay buffer as controls (37 °C, 18 h) in three biological replicates as below.

Experiment	Light Labelled	Medium Labelled	Heavy Labelled
Biological Replicate 1	assay buffer	KLK7 treated	dmKLK7 treated
Biological Replicate 2	dmKLK7 treated	assay buffer	KLK7 treated
Biological Replicate 3	KLK7 treated	dmKLK7 treated	assay buffer

Reactions were stopped by heating with the sample buffer and alkylated with iodoacetamide (IAA, 12.5 mM, RT, 1 h, light-protected, Sigma-Aldrich).

SDS-PAGE, Gel Slicing and In-gel Trypsin Digestion—Half of each treatment (10 μg) in each biological replicate was pooled and resolved on a 12% SDS-PAGE gel (supplemental Fig. S1*A*). To identify KLK7 substrates, the PROTOMAP approach was followed (10), where gel lanes were partitioned into 20 slices, then further sectioned into ~1 mm^3 pieces and pooled before drying with neat acetonitrile. In-gel trypsin digestion was performed as per Shevchenko *et al.* (18), omitting reduction and alkylation steps as these were performed before SDS-PAGE. Concentrated peptide extracts were re-suspended in 20 μl of 0.1% (v/v) formic acid containing 2% acetonitrile.

qPROTOMAP LC-MS/MS—Tryptic peptides were analyzed on a nano ACQUITY UPLC system (Waters, Milford, MA) coupled to a

[1] The abbreviations used are: ATCC, American Type Culture Collection; dmKLK7, double mutant Kallikreinrelated peptidase 7; BCA, bicinchoninic acid assay; BSA, bovine serum albumin; CM, conditioned media; COL, collagen; DPBS, Dulbecco's phosphate-buffered saline; ECM, extracellular matrix; FBS, fetal bovine serum; FDR, false discovery rate; HPG-ALD, hyper branched polyglycerol-aldehyde; IAA, iodoacetamide; IDA, Information Dependent Acquisition; IGFBP, insulin-like growth factor binding protein; IPA, ingenuity pathway analysis; MMP, matrix metalloprotease; qPROTOMAP, quantitative PROtein TOpography and Migration Analysis Platform; SILAC, stable isotopic labelling by amino acids in cell culture; TAILS, Terminal Amine Isotopic Labelling of Substrates; TPP, trans proteomics pipeline; THBS1, thrombospondin 1; UniProtKB, UniProt Knowledgebase.

TripleTOF 5600plus mass spectrometer (AB Sciex, Framingham, MA) via a Nanospray III Ion Source (AB Sciex). A sample aliquot of 5 μl was loaded onto a trap column (Symmetry C18 (5 μm) 0.18 mm x 20 mm; Waters), washed for 3 min at a rate of 15 μl/min and then separated on a BEH130 C18 column (1.7 μm, 75 μm x 200 mm; Waters) at a rate of 300 nL/min. Eluent A was 0.1% formic acid in milliQ water and eluent B was 0.1% formic acid in acetonitrile. The sample was trapped at 2% B and separated using the following gradient: 0 min (2% B) - 1 min (5% B) - 61 min (30% B) - 71 min (45% B) - 78 min (95% B) - 88 min (95% B) - 90 min (2% B) - 110 min (2% B). MS data was acquired in a data dependent manner.

The TripleTOF 5600plus mass spectrometer was operated in positive ion and high-resolution mode with an approximate resolution of 35,000. The mass window for precursor selection in the quadrupole was set to unit resolution (*m/z* 0.7 window). Parameter settings for the ion source were as follows: gas 1 = 25, gas 2 = 0, curtain gas = 25, ion spray voltage = 2300 V. Ion optics parameters were set as follows: Declustering potential = 80 V, collision energy (survey scan) = 10 V, rolling collision energy voltage was used for CID (collision-induced dissociation) fragmentation with a collision energy spread of 3. Nitrogen was used as the collision gas. Each cycle (1.3 s) consisted of a TOF-MS survey scan (mass range: 300–1800 Da, dwell time: 250 ms) followed by sequential fragmentation (mass range: 100–2000 Da, dwell time: 50 ms) of the 20 most intense precursors selected according to IDA (Information Dependent Acquisition) criteria. IDA criteria were specified as follows: Ions with *m/z* 300–1250 and charge 2–5 above a threshold of 20 cps were selected for fragmentation and excluded thereafter for 8 s. Mass spec recalibration was performed after eight hours of data acquisition using 50 fmol of a bovine serum albumin digest standard.

MS data was analyzed using MaxQuant version 1.5.0.30 (19). Each gel band analyzed was defined as a separate experiment in the experimental design section. MS/MS spectra were searched with Andromeda (20) against a SwissProt database (taxonomy: Homo sapiens; 20,267 entries, downloaded August 2013) and the MaxQuant contaminant database (247 entries) containing frequently observed contaminants such as keratins and proteases. Database searches were performed with the following search parameters: SILAC triplex labels were specified as light (Arg0Lys0), medium (Arg6Lys4) and heavy (Arg10Lys8). Strict enzyme specificity was required for trypsin with two missed cleavages allowed. Variable modifications included M oxidation (+ 15.994919), N and Q deamidation (+ 0.984016) and N-terminal acetylation of proteins (+ 42.010565). Carbamidomethylation of C (+ 57.021464) was set to fixed modification. AB Sciex TOF was set as instrument type using default settings. Precursor tolerance was set to 0.07 Da and 0.006 Da for the first and main search, respectively. Fragment tolerance was set at 40 ppm. False discovery rates (FDRs) at the peptide and protein levels were fixed at 1%. Quantitation was based on unique peptides only and a minimum of two ratio counts was required. The requantification feature was enabled.

Peptograph Generation and Analysis—The MaxQuant "txt" results files were further processed and quantitative peptographs were created with in-house Perl scripts generated based on qPROTOMAP from Dix *et al.* (21). In brief, cleaved proteins were identified based on the distribution of peptide ratios in each band. The distribution of peptide ratios in each band were organized into quartiles. The band was flagged as control specific, indicative of a parental degradation event, if the ratios in the upper three quartiles were more than 3-fold elevated in the control sample. The band was flagged as KLK7 specific, indicative of a cleaved fragment, if the ratios in the lower three quartiles were more than 3-fold elevated in the KLK7-treated samples. At this stage, peptides with MaxQuant score <40 or Posterior Error Probability (PEP) >0.05 and MaxQuant score <60 and PEP >0.01 were not included in the peptographs. Peptographs of those proteins with cell surface or extracellular localization, as denoted by Ingenuity Pathway Analysis software (IPA, Qiagen), were interrogated for evidence of KLK7-mediated proteolysis. A description of the peptograph interpretation can be found in supplemental Fig. S2. Peptographs were assessed to identify putative KLK7 substrates in KLK7-treated *versus* buffer control as no cleavages were observed in the dmKLK7-treated compared with the buffer control. Briefly, a protein to be considered a putative KLK7 substrate, KLK7-generated protein fragments were required to be abundantly identified in the KLK7-treated group; *i.e.* have a log2 SILAC label ratio ≥ 2 compared with the buffer-treated group, isolated from a single gel slice. In addition, only one KLK7-generated product was required for the protein to be considered a putative KLK7 substrate, although many KLK7 substrates were identified with multiple KLK7-generated protein fragments.

Screening for cleavage sites of qPROTOMAP-identified putative KLK7 substrates in ovarian cancer representative cell secretions using TAILS—

Treating Cell Conditioned Media with KLK7 and dmKLK7—CM (200 μg) was treated with either KLK7, dmKLK7 (1:200; active site-titrated KLK7: CM; *w/w*) or assay buffer as controls (37 °C, 18 h) in three biological replicates (supplemental Fig. S1*B*). The reaction was quenched (1 M guanidine hydrochloride, 5 mM DTT; boiling 5–10 min), followed by alkylation (chloroacetamide 12 mM, RT, 30 min, light-protected).

TAILS Sample Preparation—Samples were prepared as described (22) with a few modifications as given below. The labeling reaction was quenched by adding 100 mM glycine and vortexing (RT, 30 min). Pooled samples were trypsin digested (supplemental Fig. S1*C*) and desalted using the Oasis HLB cartridges (Waters, United Kingdom) as per manufacturer's instructions. The peptide samples were depleted of the HPG-ALD polymer (available through www.flintbox.ca) by using the C18 StageTips, which were preconditioned by forcing 100 μl of 100% methanol through the disks with a syringe fitted to the end of the pipette tip. Any remaining organic solvent was removed from the column by forcing through 100 μl of buffer A (0.1% formic acid in milliQ water or acidified water) twice. The acidified peptide sample (pH <3.5) was forced through the column three times followed by two washes with buffer A. Peptides were eluted with 40 μl of buffer B (0.1% formic acid, 80% acetonitrile in water), vacuum dried and re-dissolved in 2% ACN, 0.1% formic acid by sonicating for 10 min and spin-vortexing for another 10 min.

TAILS LC-MS/MS—In brief, the resulting peptides were analyzed by LC-MS/MS using the Q Exactive mass spectrometer (Thermo Scientific, Bremen, Germany) coupled online with a RSLC nano UPLC (Ultimate 3000, Thermo Scientific). Samples were loaded on a nanoViper PepMap100 C18 trap column (100 μm × 2 cm) in 2% (v/v) acetonitrile/0.1% (v/v) formic acid, at a flow rate of 15 μl/min. Peptides were eluted and separated at a flow rate of 250 μl/min on a PepMap C18 nanocolumn (3 μm 100 Å pore size, 75 μm × 50 cm, Thermo), where acetonitrile was elevated from 2% (v/v) to 8% (v/v) over 1 min, followed with a linear acetonitrile gradient from 8% (v/v) to 24% (v/v) in 0.1% (v/v) formic acid for 24 min, followed by a linear increase to 30% (v/v) acetonitrile in 0.1% (v/v) formic acid over 3 min, an additional increase up to 80% (v/v) acetonitrile in 0.1% (v/v) formic acid over 3 min, followed by reduction of acetonitrile back to 2% (v/v) and re-equilibration. The eluent was nebulized and ionized using a Thermo nano electrospray source with a distal coated fused silica emitter (New Objective, Woburn, MA). Typical mass spectrometric conditions were as follows: spray voltage, 1.7 kV; no sheath and auxiliary gas flow; heated capillary temperature, 275 °C.

The Q Exactive instrument was operated in the data dependent mode to automatically switch between full scan MS and MS/MS

acquisition. Survey full scan MS spectra (*m/z* 375–1800) were acquired in the Orbitrap with 70,000 resolution (*m/z* 200) after accumulation of ions to a 3×10^6 target value with maximum injection time of 30 ms. Dynamic exclusion was set to 15 s. The 10 most intense multiply charged ions ($z \geq 2$) were sequentially isolated and fragmented in the octopole collision cell by higher energy collision dissociation (HCD, normalized collision energy 27%) with a maximum injection time of 60 ms. MS/MS spectra were acquired in the Orbitrap with 17,500 resolution, automatic gain control target of 5×10^4 counts and 2.0 Da isolation width. Underfill ratio was at 1%.

TAILS Data Analysis—Spectra were converted to mzXML files using MSconvert (Profile setting, facilitated by ProteoWizard release 3.0.9134 (23), and were searched using X!Tandem [release 2009.10.01.1 LabKey, Insilicos, Institute for Systems Biology, (24)] contained within the TPP [v4.6; (25)] with high-resolution k-score against the UniProt Knowledgebase (UniProtKB) human protein database [Released February 2015; SwissProt 42077 entries (26)] supplemented with known contaminants [cRAP database released Feb 2012; 115 entries (27)]. Reverse sequences (Decoys) informed false positive identification frequency. Search parameters were as follows: precursor ion mass (monoisotopic) tolerance ± 20 ppm; MS/MS tolerance ± 0.02 Da; and semi-Arg-C cleavage allowing for up to one missed cleavage. Fixed modifications included C carbamidomethylation (+ 57.021464) and light dimethylation (+ 28.031300) of N termini and K residues. Variable modifications included M oxidation (+ 15.994919) and the mass difference of H and L dimethylation (+ 6.031817) for N termini and K residues. Peptide Prophet (v4.6) was used to curate peptide-spectrum matches of FDR ≤ 1% and assign representative proteins/protein isoforms. XPRESS software (28) within the TPP was used for relative quantification of H : L peptide ratios.

Peptide analysis was performed according to Kleifeld *et al.* (22). Briefly, for TAILS-identified peptides in each replicate, mean for the log2 (H:L) values in "XPRESS" column was calculated and that value was subtracted from log2(H:L) ratios calculated for each peptide in the data set. Histogram of the log2-ratios was plotted to check for normal distribution and deviation from the expected center at 0 using Wessa.net73 (http://www.wessa.net/rwasp_fitdistrnorm.wasp) (supplemental Fig. S3). The standard deviation of the corrected log2 ratios for natural N termini was calculated and peptides with the corrected log2(H:L) ratios that are higher than three times the standard deviation (*i.e.* Log2 (H:L) ≥ 2) are considered to be high-probability substrates of the protease of interest in the substrate with a cleavage site as identified by the neo-N-terminal peptide. KLK7-generated neo-N termini were selected if (a) Log2 (H:L) ≥ 2; (b) identified by at least two spectra or in at least two replicates (with different variable modifications included) (29); and (c) annotated to be extracellular or of cell surface origin in the Ingenuity Pathway Analysis (IPA). Data from each of three biological replicates was analyzed independent of other replicates.

The KLK7 cleavage site specificity profile, based on TAILS-identified cleavage events within all putative KLK7 substrates, was generated using iceLogo (https://iomics.ugent.be/icelogoserver/). Annotation of domains and binding/interaction regions spanning the identified KLK7 cleavage sites, as annotated in the UniProtKB, was performed using TopFINDer [TopFIND 3.0; (30)]. Biological process annotations in the Gene Ontology Database that were significantly associated with putative KLK7 substrates identified by both qPROTOMAP and TAILS were calculated using a modified Fisher Exact test embedded in the functional annotation tool provided by The Database for Annotation, Visualization and Integrated Discovery (DAVID) v6.7 (31).

Validation of KLK7-mediated Proteolysis of Selected Substrates Identified in Both Proteomics Platforms—*Recombinant Protein Digestion and SDS-PAGE/Silver Staining or Western Blotting Analyses*—Human recombinant proteins of THBS1 (Merck, NSW, Australia), pro-MMP10, pro-MMP1 (R&D Systems, Minneapolis, MN) and IGFBP6 (Thermo Fisher Scientific, VIC, Australia) were digested with KLK7 in assay buffer (37 °C/18 h) using 1:10–1000 molar ratios (similar to ~1:50–5000 *w/w* ratios) of active site-titrated KLK7: substrate. As controls, recombinant proteins were treated with buffer or dmKLK7 to the highest concentration of KLK7, and KLK7 or dmKLK7 also were incubated alone (37 °C/18 h) to distinguish any bands generated by auto-degradation of the enzymes. Reactions were terminated and reduced by boiling with Laemmli sample buffer containing β-mercaptoethanol. Samples were resolved by SDS-PAGE and visualized by silver staining. Western blot analysis was also performed on respective KLK7-treated recombinant proteins or CM with antibodies targeting THBS1 (full length: ab1823, Abcam, Cambridge, MA; N-20: sc-12312, Santa Cruz, California), MMP1 (full length: ab89767, Abcam), KLK7 (32), MMP2 (amino acids 475–490: ab37150, Abcam) and IGFBP6 (amino acids 128–141 of human IGFBP6, ab109765, Abcam).

MMP10 Activity Assay—Pro-MMP10 was treated with KLK7 (1:100 molar ratio; active site-titrated KLK7:pro-MMP10) or assay buffer or equivalent concentrations of dmKLK7 as controls (37 °C/18 h). Relative fluorescence units (RFU) was measured after adding Mca-R-P-K-P-V-E-Nval-W-R-K(Dnp)-NH_2, the MMP10-specific peptide substrate (10 μM; R&D Systems) in MMP10 assay buffer using a X-Mark Micro plate Spectrophotometer (Bio-Rad, Philadelphia, PA; Ex. 320 nm, Em. 405 nm, 37 °C). A blank sample, consisting only of MMP10 assay buffer and peptide substrate, served as a background control. RFU of all samples were corrected for RFU of the blank at 0 s. Results presented correspond to mean of corrected RFU obtained in nine technical replicates.

Confirmation of IGFBP6 Cleavage Site—Recombinant IGFBP6 was incubated with active KLK7 (active site-titrated KLK7:IGFBP6 = 1:50 molar ratio) for 18 h at 37 °C in KLK7 activity buffer. Protein mixture was loaded on C18 column (A5700310 OMIX, 96 C18 10 μl from Agilent Technologies Australia, VIC, Australia) and N termini demethylated with Formaldehyde. After washes and elution, proteins were trypsin digested overnight at 37 °C (ratio trypsin/protein of 1:10, Promega Sequencing grade Trypsin (V5111)). Peptides were cleaned using C18 column and analyzed on an Easy nLC - Q Exactive Plus (configurations are as above). MS data have been analyzed using Proteome Discoverer 2.2.0.388 (Thermo Scientific). MS/MS spectra were searched with Sequest HT engine against a SwissProt database (Homo Sapiens, 20,153 sequences). Database search was performed with the following search parameters: semi-trypsin peptides with two missed cleavages allowed, variable modifications included M oxidation (+ 15.994 Da), N-terminal acetylation (+ 42.010 Da) and N-terminal Dimethylation (+28.031 Da). Carbamidomethylation of C (+ 57.021 Da) and Dimethylation of K (+28.031 Da) were set to fixed modification. Precursor tolerance was set to 10 ppm and fragment tolerance was set at 0.02 Da. False discovery rates (FDRs) at the peptide and protein levels were fixed at 1%.

RESULTS

Novel Putative KLK7 Substrates Were Identified in SKOV-3 Cell CM by qPROTOMAP—Eighty-seven proteins were determined to be putative extracellular KLK7 substrates among a total of 261 putative substrates identified across all three samples (Table I, supplemental Table S1). Notably, established KLK7 substrates, fibronectin 1 (FN1), desmoglein 2 (DSG2, (33)) and matrix metalloprotease 2 (MMP2, (34)) were also cleaved in SKOV-3 cell CM herein, validating the

TABLE I
Eighty-seven putative extracellular KLK7 substrates identified in the qPROTOMAP analysis of SKOV-3 cell conditioned media

Accession	Description	Protein Length(AA)	Protein Size (kDa)	Protein Coverage (%)	Unique Peptides
O00468	Agrin	2045	214.8	40.8	61
P61160	Actin-related protein 2	394	44.8	18	7
P61158	Actin-related protein 3	418	47.4	29.2	12
P04083	Annexin A1	346	38.7	68.5	28
P08133	Annexin A6	673	75.9	21.1	13
P05067	Amyloid beta A4 protein	770	86.9	35.5	24
P30530	Tyrosine-protein kinase receptor UFO	894	98.3	7.3	5
Q6YHK3	CD109 antigen	1445	161.7	11.7	16
P55285	Cadherin-6	790	88.3	9	7
P00751	Complement factor B	764	85.5	23.3	17
Q9Y696	Chloride intracellular channel protein 4	253	28.8	67.6	16
O94985	Calsyntenin-1	981	109.8	39.8	37
Q00610	Clathrin heavy chain 1	1675	191.6	38	55
Q99715	Collagen alpha-1(XII) chain	3063	333.1	52.9	153
P39060	Collagen alpha-1(XVIII) chain	1754	178.2	17	24
P02452	Collagen alpha-1(I) chain	1464	138.9	13.9	17
P02462	Collagen alpha-1(IV) chain	1669	160.6	9.6	10
P08572	Collagen alpha-2(IV) chain	1712	167.6	10.5	13
P20908	Collagen alpha-1(V) chain	1838	183.6	13.6	19
P12109	Collagen alpha-1(VI) chain	1028	108.5	17.7	15
P12110	Collagen alpha-2(VI) chain	1019	108.6	9	10
Q02388	Collagen alpha-1(VII) chain	2944	295.2	16.8	37
P00450	Ceruloplasmin	1065	122.2	10.3	9
O00622	Protein CYR61	381	42	17.1	6
Q14118	Dystroglycan	895	97.4	22	16
Q9UBP4	Dickkopf-related protein 3	350	38.4	28	7
*Q14126	Desmoglein-2	1118	122.3	3.8	3
Q16610	Extracellular matrix protein 1	540	60.7	26.3	13
O43854	EGF-like repeat and discoidin I-like domain	480	53.8	36	18
P20827	Ephrin-A1	205	23.8	7.3	2
P15311	Ezrin	586	69.4	41.1	25
Q92520	Protein FAM3C	227	24.7	50.2	10
P23142	Fibulin-1	703	77.2	19.9	10
P98095	Fibulin-2	1184	126.6	24.5	22
P35555	Fibrillin-1	2871	312.2	20.4	51
Q14512	Fibroblast growth factor-binding protein 1	234	26.3	23.9	6
*P02751	Fibronectin	2386	262.6	36.1	66
Q12841	Follistatin-related protein 1	308	35	69.2	27
O95633	Follistatin-related protein 3	263	27.7	17.1	4
Q14393	Growth arrest-specific protein 6	721	79.7	9.2	5
P56159	GDNF family receptor alpha-1	465	51.5	11	5
P35052	Glypican-1	558	61.7	41.9	18
P28799	Granulins	593	63.5	30.5	16
P06396	Gelsolin	782	85.7	16.2	9
P98160	Basement membrane-specific heparan sulfate protein	4391	468.8	34.2	110
Q92743	Serine protease HTRA1	480	51.3	22.1	12
P18065	Insulin-like growth factor-binding protein 2	325	34.8	30.8	9
Q16270	Insulin-like growth factor-binding protein 7	282	29.1	57.8	20
P26006	Integrin alpha-3	1051	116.6	8.8	10
P55268	Laminin subunit beta-2	1798	196	30	42
P11047	Laminin subunit gamma-1	1609	177.6	48.9	73
P09382	Galectin-1	135	14.7	64.4	10
Q08380	Galectin-3-binding protein	585	65.3	40.9	19
Q9Y4K0	Lysyl oxidase homolog 2	774	86.7	28.3	19
Q8N2S1	Latent-transforming growth factor beta-binding protein 4	1624	173.4	6.3	9
O00339	Matrilin-2	956	106.8	12.9	10
P08581	Hepatocyte growth factor receptor	1390	155.5	12.1	14
P03956	Interstitial collagenase	469	54	50.1	30

TABLE I—*continued*

Accession	Description	Protein Length(AA)	Protein Size (kDa)	Protein Coverage (%)	Unique Peptides
P09238	Stromelysin-2	476	54.2	26.5	14
*P08253	72 kDa type IV collagenase	660	73.9	24.4	14
P26038	Moesin	577	67.8	48	31
Q14112	Nidogen-2	1375	151.3	40	40
P48745	Protein NOV homolog	357	39.2	37.3	11
P19021	Peptidyl-glycine alpha-amidating monooxygenase	973	108.3	11	11
Q8NBP7	Proprotein convertase subtilisin/kexin type	692	74.3	22.8	13
Q9NRA1	Platelet-derived growth factor C	345	39	18	7
P00749	Urokinase-type plasminogen activator	431	48.5	52.9	21
P07225	Vitamin K-dependent protein S	676	75.1	13.3	10
P07602	Prosaposin	524	58.1	39.9	17
P10586	Receptor-type tyrosine-protein phosphatase F	1907	212.9	23.7	35
Q13332	Receptor-type tyrosine-protein phosphatase S	1948	217	17.3	23
Q92626	Peroxidasin homolog	1479	165.3	38.6	49
P63000	Ras-related C3 botulinum toxin substrate 1	192	21.5	25	5
O00560	Syntenin-1	298	32.4	44.6	10
P05121	Plasminogen activator inhibitor 1	402	45.1	34.6	14
P50454	Serpin H1	418	46.4	41.4	10
P09486	SPARC	303	34.6	31	11
Q13813	Spectrin alpha chain, non-erythrocytic 1	2472	284.5	36.7	79
Q01082	Spectrin beta chain, non-erythrocytic 1	2364	274.6	32.1	63
P52823	Stanniocalcin-1	247	27.6	34	9
Q15582	Transforming growth factor-beta-induced protein	683	74.7	43.5	26
P07996	Thrombospondin-1	1170	129.4	15.9	14
P16035	Metalloproteinase inhibitor 2	220	24.4	62.3	18
Q9Y490	Talin-1	2541	269.8	23.6	42
Q99536	Synaptic vesicle membrane protein VAT-1 homolog	393	41.9	8.7	3
P13611	Versican core protein	3396	372.8	6.8	23
P18206	Vinculin	1134	123.8	49.1	52

Accession, reviewed UniProtKB accession; Description, UniProtKB protein description; *Established KLK7 substrates.

qPROTOMAP approach. The remaining other 84 KLK7 substrates have not been determined as ovarian cancer cell-derived KLK7 substrates by other published work, and thus are deemed novel putative KLK7 substrates. Some are established substrates of other KLKs, thus their determination as KLK7 substrates was not unexpected. These include basement or extracellular matrix proteins, such as collagen I and IV, and other proteins, such as amyloid beta (A4) precursor protein (APP), IGFBP2, thrombospondin 1 (THBS1), and vinculin (VCL). Thus, apart from the established KLK7 substrates, FN1, DSG2, and MMP2 and the six above known to be cleaved by other KLKs, KLK7 cleaved an additional 78 novel substrates.

TAILS Approach Identifies Exact Cleavage Sites Of qPROTOMAP-identified Putative KLK7 Substrates—To determine the exact cleavage sites of the qPROTOMAP-identified substrates TAILS analysis was employed with a lower KLK7:CM ratio (1:200), thereby allowing for identification of precise KLK7 cleavage sites. However, pre-TAILS analysis was not performed; putative cleavage site identification was limited to proteins that have been already identified in the qPROTOMAP approach. This analysis identified cleavage sites for 18 putative KLK7 substrates (Table II, supplemental Table S2). Notably, two established KLK7 substrates, MMP2 (34) and IGFBP3 (35) were cleaved in SKOV-3 cell CM, in the TAILS approach. Moreover, the two established substrates of KLK7 that were identified in the qPROTOMAP approach, DSG2 and FN1, were not detected to be cleaved by KLK7 in the TAILS approach where a 4-fold less concentration (1:200 of active site-titrated KLK7: CM *w/w*) of KLK7 was used compared with the qPROTOMAP approach (1:50 of active site-titrated KLK7: CM *w/w*).

KLK7 Hydrolyzes Substrates Into Bio-active Products—In the current study, three (calsyntenin-1, MMP10 and thrombospondin 1) of the 16 putative KLK7 substrates were identified to be hydrolyzed by KLK7 to produce potential bioactive by products (Table III) as in UniProtKB. Herein, KLK7-mediated hydrolysis of MMP10 and thrombospondin 1 was further assessed, as KLK7-generated bioactive fragments of these proteins have a high likelihood of exerting cancer promoting functions according to the literature. Interestingly, MMP1 which was also identified as a substrate of KLK7 could only be validated on Western blot analysis of SKOV-3 CM and not with recombinant proteins (supplemental Fig. S4).

KLK7 Directly Activates pro-MMP10—Pro-MMP10 was identified as a substrate of KLK7 in the qPROTOMAP and TAILS analysis of SKOV-3 cell CM. Peptides derived from pro-MMP10 were identified in both the control and KLK7-

TABLE II
Eighteen putative extracellular KLK7 substrates identified in the TAILS analysis of SKOV-3 cell conditioned media

Accession	Symbol	Protein Description	P1	Peptides	*m/z*	Precursor charge	Probability
Peptidases and peptidase regulators							
#P03956	MMP1	Matrix metallopeptidase 1	70	F.FGLKVTGKPDAETLKVMKQPR.C	838.5505	3	1
			71	F.GLKVTGKPDAETLKVMKQPR.C	789.5278	3	1
			116	Y.RIENYTPDLPR.A	469.9315	3	0.9889
			149	F.SGDVQLAQDDIDGIQAIYGR.S	723.3728	3	1
*#P08253	MMP2	Matrix metallopeptidase 2	80	F.FGLPQTGDLDQNTIETMR.K	1035.5226	2	1
#P09238	MMP10	Matrix metallopeptidase 10	99	F.SSFPGMPKWR.K	420.9112	3	1
Pathway inhibitors							
#Q9UBP4	DKK3	Dickkopf WNT signaling pathway inhibitor 3	128	F.SETVITSVGDEEGRR.S	834.9341	2	0.9987
ECM/basement membrane constituents and ECM/ growth factor regulators							
#Q02388	COL7A1	Collagen, type VII, alpha 1	2819	Y.AADTAGSQLHAVPVLR.V	547.3162	3	0.9991
#Q99715	COL12A1	Collagen, type XII, alpha 1	1139	D.NTVVLEELR.A	553.8351	2	0.9452
			1138	Y.DNTVVLEELR.A	611.3486	2	0.9986
			2926	M.LNQIPNDYQSSR.N	734.8836	2	0.9924
#P35555	FBN1	Fibrillin 1	1760	Y.TGLPVDIDECR.E	654.8376	2	0.9998
#O95633	FSTL3	Follistatin-like 3	84	L.GFLGLVHCLPCKDSCDGVECGPGKACR.M	1051.1868	3	1
*P17936	IGFBP3	Insulin-like growth factor binding protein 3	186	Y.KVDYESQSTDTQNFSSESKR.E	813.4225	3	1
P24592	IGFBP6	Insulin-like growth factor binding protein 6	165	R.HLDSVLQQLQTEVYR.G	932.0126	2	1
			179	Y.RGAQTLYVPNCDHR.G	860.9416	2	0.8584
#Q14112	NID2	Nidogen 2 (osteonidogen)	80	N.GIISTQDFPR.E	584.3326	2	0.8835
			124	Y.REDTSPAVLGLAAR.Y	745.4311	2	0.9988
#P09486	SPARC	Secreted protein, acidic, cysteine-rich (osteonectin)	179	Y.ERDEDNNLLTEKQKLR.V	1052.1161	2	0.918
#P07996	THBS1	Thrombospondin 1	258	Y.IGHKTKDLQAICGISCDELSSMVLELR.G	1059.2505	3	1
			665	Y.LGHYSDPMYR.C	636.8161	2	0.9809
Cell adhesion molecules/regulators and signal transducers							
#P55285	CDH6	Cadherin 6, type 2, K-cadherin	343	Y.TLKVEASNPYVEPR.F	835.9911	2	0.9999
Cytoskeletal proteins/regulators							
#P15311	EZR	Ezrin	424	Y.TAKIALLEEAR.R	641.9221	2	0.9972
Other (Ion channel, galactoside/carbohydrate binding and immunomodulatory proteins)							
#O94985	CLSTN1	Calsyntenin 1	169	Y.KATVIEGKQYDSILR.V	912.0781	2	0.9999
#Q08380	LGALS3BP	Lectin, galactoside-binding, soluble, 3 binding protein	442	Y.SSDYFQAPSDYR.Y	735.3416	2	0.9975
#P07602	PSAP	Prosaposin	171	F.MANIPLLLYPQDGPR.S	866.4871	2	0.9998

Accession, reviewed UniProt KB accession; Symbol, UniProtKB/Swiss-Prot entry name prefix (all_HUMAN) with HUGO gene name for UniProtKB entries; Protein Description, UniProtKB protein description; P1, KLK7 cleaves C-terminal to; Peptides, TAILS-identified peptide cleavage sites with the "." representing where the cleavage is identified; *Established KLK7 substrates.

TABLE III
Putative KLK7 substrates that may have hydrolyzed into bioactive by-products by KLK7 proteolysis in SKOV-3 cell conditioned media, as in UniProtKB

Description	Putative KLK7 cleavage product/chain	Annotated cleavage product bioactivity in UniProtKB
Calsyntenin-1	A fragment of soluble calsyntenin alpha	None annotated
Matrix metallopeptidase 10 (stromelysin 2)	Stromelysin 2	Peptidase
Thrombospondin 1	N-terminal heparin binding domain	Regulation of angiogenesis

Description, UniProtKB protein description.

treated conditions (Fig. 1*A* and 1*C*, See supplementary Fig. S2 for peptograph description). In gel slices 6 and 7 at ~55 kDa three protein fragments representing the full length pro-MMP10 were identified (blue). Protein fragments representative of the active MMP10 were retrieved in the control sample to a lesser extent, indicating that MMP10 remains in its inactive form in the control sample. In contrast, in the KLK7-treated condition (red), a larger number of protein fragments, representative of active MMP10, at ~45 kDa (gel slice 11), were identified with high confidence showing much higher abundance in the KLK7-treated sample (Log2 KLK7/control = 2–5). Further in the KLK7-treated condition, two peptides in gel slice 20 were identified, which may have been the result of auto-cleavage of MMP10 post activation, or potential cleavage by another protease in the cell CM. Intriguingly, pro-MMP10 was also recognized as a substrate of KLK7 in the TAILS analysis. Only one cleavage site was identified cleaving C-terminal to phenylalanine^{99} ($F^{99}\downarrow$SSFPGMPKWR; Log2 KLK7/control = 4.32, 20-fold higher in the KLK7-treated condition) suggesting KLK7-mediated cleavage following the activation peptide, that spans from the residue 18 to 98 (Fig. 1*A* and 1*B*) of the prepro-MMP10. Further, the identified cleavage site ($F^{99}\downarrow$SSFPGMPKWR), as shown by the TAILS analysis, suggests direct cleavage of pro-MMP10 by KLK7, noting the chymotryptic-like activity of KLK7 (15, 36).

On biochemical validation (Fig. 1*D*), KLK7 completely degraded the pro-MMP10 band at 54 kDa (1:10 molar ratio, lane 2), generating 45 kDa active MMP10 protein, as noted by an increase in intensity compared with lane 1. To further assess the direct activation of pro-MMP10 by KLK7, a peptide substrate assay was performed. KLK7-treated pro-MMP10 showed a clear increase in RFU over time compared with that of the dmKLK7-treated pro-MMP10 or pro-MMP10 alone, indicating KLK7-mediated activation of pro-MMP10 (Fig. 1*E*, 1*F*).

KLK7 liberates the N terminus of THBS1—THBS1 was identified as a substrate of KLK7 in the qPROTOMAP and TAILS analysis of SKOV-3 cell CM. Peptides representing THBS1 were identified in both the control and KLK7-treated conditions, with a high number of high molecular weight peptides identified in the former (Fig. 2*A* and 2*C*, See supplemental Fig. S2 for peptograph description). In the control group (blue), THBS1 protein fragments were identified in the gel slices 2 and 3, representing full length THBS1 (150 kDa). In the KLK7-treated condition (red), N-terminal THBS1 fragments spanning the heparin binding domain (H) were identified in the gel slices 11, 12, and 13 (26–28 kDa) and also peptides spanning the von Willebrand factor-type C (VWFC) domain, THBS1-like domain 1 (THBS-1) and the EGF-like domains (E) were identified in gel slices 5–6 representing a 75–100 kDa fragment.

The TAILS analysis confirmed qPROTOMAP observations by identifying two peptides representing KLK7-mediated cleavage of THBS1 at two distinct sites. The peptide depicting the cleavage of THBS1 after tyrosine (Y^{258}) $Y^{258}\downarrow$IGHKTKD-LQAICGISCDELSSMVLER (Fig. 2*A* and 2*B*; Log2 KLK7/control = 9.96) possibly generates an N-terminal 28 kDa fragment containing the heparin binding domain. The second cleavage site was identified C-terminal to Y^{665} ($Y^{665}\downarrow$LGHYSDPMYR), suggesting a cleavage in the EGF-like 2 domain generating a C-terminal THBS-like domain 3 (THBS-3) and THBS C-terminal (THBS-C) containing fragment and a fragment containing the Von Willebrand Factor-type C (VWFC) domain, THBS-1 and the EGF-like domains (E), in accordance with the qPROTOMAP observation.

In the biochemical validation (Fig. 2*D*), KLK7 hydrolyzed rTHBS1 at molar ratios of 1/10 1/50, and 1/100 and to a lesser extent at the 1/1000 molar ratio generating 130 kDa and 28 kDa fragments. Importantly, the 28 kDa and 130 kDa fragments were of high intensity, reflecting KLK7-mediated liberation of an N-terminal smaller fragment and another higher molecular weight mid-terminal fragment. The above observations were further validated by performing Western blot analysis using antibodies targeting the full length (Fig. 2*E*) and N-terminal sequence (Fig. 2*F*) of THBS1.

Heterogeneity of Cell Secreted Proteins Identified in Ovarian Cancer Cell Lines—TAILS analysis of the OVMZ-6 cell secretome identified 37 putative extracellular KLK7 substrates (Table IV, supplemental Table S3). Interestingly, on comparison of the TAILS analyses of the SKOV-3 and OVMZ-6 cell secretomes to determine any heterogeneity between the cell lines, only eight putative extracellular KLK7 substrates were identified in both SKOV-3 and OVMZ-6 cell CM. These substrates included calsyntenin-1 (CLSTN1), cystatin-C (CST3), dickkopf-related protein 3 (DKK3), ezrin (EZR), insulin-like growth factor-binding protein 6 (IGFBP6), lectin, galactoside-binding, soluble, 3 binding protein (LGALS3BP), prosaposin (PSAP) and osteonectin (SPARC) (Table IV, proteins denoted with a #). Moreover, comparison of the

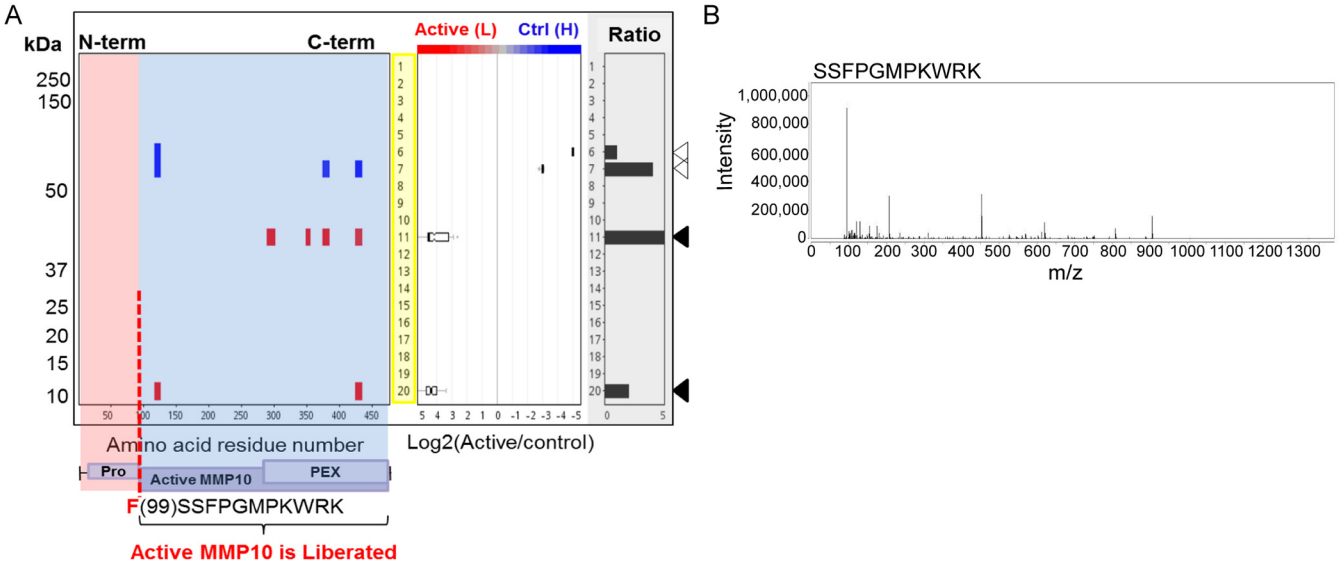

C

Peptide	Position	PEP	Score	PSMs	6			7			11			20		
					L/H	Count	Log2	L/H	Count	Log2	L/H	Count	Log2	L/H	Count	Log2
IVNYTPDLPR	117-126	6.4141E-08	148.56	8	-	0	[-5]	0.11	1	-3.1				-	0	[5]
CDPALSFDAISTLR	289-302	6.4217E-13	127.03	6							22.95	2	4.5			
DTVFIFK	349-355	0.0033558	158.12	3							52.24	1	5.7			
GIHTLGFPPTIR	374-385	0.0040072	60.255	6				0.15	1	-2.8	9.24	1	3.2			
LIADDFPGVEPK	424-435	2.4508E-06	108.68	13				0.12	2	-3.0	6.02	1	2.6	12.45	1	3.6

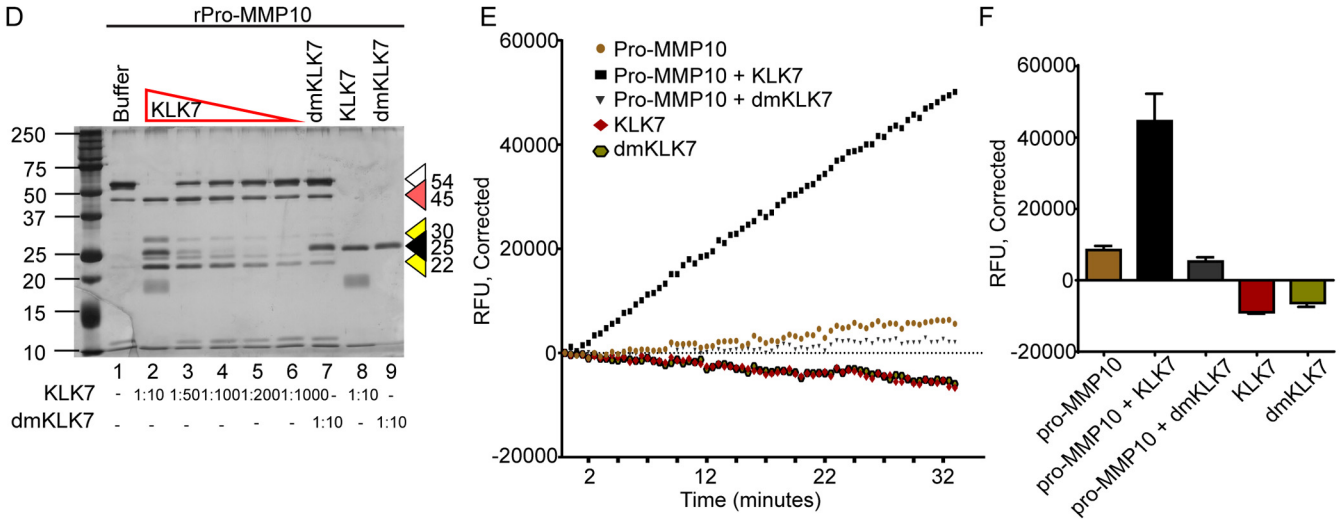

FIG. 1. **KLK7 directly activates pro-MMP10.** *A*, Peptograph (replicate 2) representing KLK7-mediated hydrolysis of pro-MMP10 in SKOV-3 cell CM. See supplemental Fig. S2 for peptograph description. The higher molecular weight (MW) peptides (blue - Heavy labeled) in gel slice 7 (Log2 KLK7/control = −3 to −5) represent the full length pro-MMP10 identified in the buffer-treated sample. The lower MW fragments in gel slices 11 and 20 (Log2 KLK7/control = 3 to 5) represent the KLK7 cleavage fragments identified in the KLK7-treated sample (red - Light labeled). A schematic of selected protein domains, based on annotation in the UniProtKB, is shown beneath the X-axis (purple boxes), aligned with the appropriate residues. Pro, activation peptide; PEX, hemopexin domain; the molecular weight of the protein standard (kDa) is indicated to the left. Arrow heads in colors depict, open: pro-MMP10 full length; black, KLK7-generated MMP10 fragments. The box plot in the middle panel represents the distribution of ratios found in each gel slice. *B*, Spectrum for the TAILS identified KLK7 cleavage site C-terminal to F^{99} and is also shown beneath the domain structure in a red dotted vertical line in *A*. *C*, Peptides identified in the qPROTOMAP analysis in gel slices 6, 7, 11 and 20 (PEP, posterior error probability; Score, the sum of the ion scores of all peptides identified; PSMs, peptide spectrum matches)

qPROTOMAP and TAILS-identified substrates in SKOV-3 and OVMZ-6 cells, respectively, revealed another seven substrates exclusive to the nine common substrates listed above (Table IV, see proteins denoted with a ¥), increasing the list of common substrates to 16. Of these sixteen commonly identified substrates we sought to further biochemically validate IGFBP6, an established substrate of KLK4 and KLK5 (37), cleavage of which is known to activate IGF signaling and enhance cancer cell proliferation (38). Notably, the established KLK7 substrate, midkine (MDK) was cleaved in OVMZ-6 cell CM.

KLK7-mediated Cleavage of IGFBP6—Cleavage C-terminal to Y^{179} was detected in both SKOV-3 and OVMZ-6 cell lines ($Y^{179}\downarrow$RGAQTLYVPNCDHRG [Log2 KLK7/control = 9.96 in OVMZ-6]). In SKOV-3 TAILS analysis two cleavages cleaving C-terminal to arginine (R)^{165} and Y^{179} ($R^{165}\downarrow$HLDSVLQQLQTEVYRG [Log2 KLK7/control = 2.94] and $Y^{179}\downarrow$RGAQTLYVPNCD HRG [Log2 KLK7/control = 4.64]) were identified (Fig. 3*A* and 3*B*). However, in OVMZ-6 cell CM, two cleavages additional to the above were detected cleaving C-terminal to G^{219} and M^{218} ($G^{219}\downarrow$KSLPGSPDGNGSSSCPTGSSG [Log2 KLK7/control = 9.96], $M^{218}\downarrow$GKSLPGSPDGN GSSSCPTGSSG [-log2 = 4.64]). This observation suggests that other individually identified cleavage sites, such as G^{219} and M^{218} are potentially differentially influenced by other factors in these two cell lines or missed cleavages by trypsin. Further, the identified cleavage sites display either KLK7-mediated direct cleavages of IGFBP6 or indirect cleavages, as noted by the chymotryptic- (Y^{179}) or tryptic-like (R^{165}) cleavages and other cleavage specificities, such as G^{219} respectively.

In the biochemical validation (Fig. 3*C*), KLK7 hydrolyzed rIGFBP6 at molar ratios of 1/10 1/50, and 1/100 molar ratio generating a 10 kDa fragment. For further verification, KLK7-generated major cleavage product of 10 kDa was sequenced to identify the primary KLK7 cleavage site on IGFBP6. This analysis revealed that the Y^{179} is the most abundant N-terminal apart from the natural N terminus of IGFBP6 (RCPGCGQGVQAGCPGGCVEEEDGGSPAEGCAEAEGCLRR peptide) (Table V), further verifying the TAILS-identified cleavage site. Apart from the Y^{179} cleavage site, R^{165} cleavage was also identified with low abundance, although a fragment representing this cleavage had not been observed in the biochemical validation.

Annotated Cellular Processes of the Identified Putative Extracellular KLK7 Substrates in SKOV-3 and OVMZ-6 Cell CM—Putative extracellular KLK7 substrates identified in both cell lines are predicted to be primarily involved in cell-cell adhesion, extracellular matrix organization, and cell surface receptor-linked signal transduction gene ontology (GO)-annotated biological processes (Table VI, supplemental Table S4–S5), equivalent to the established functions of KLK7. The GO analysis revealed that, albeit the differences in the secreted proteome of these two cell lines, KLK7 exerts similar functional roles by cleaving extracellular and membrane proteins involved in these processes.

TAILS Analysis Determined A Chymotryptic-like Cleavage Specificity Profile for KLK7—The KLK7 cleavage site specificity profile (Fig. 4*A*), based on TAILS-identified cleavage events within all putative KLK7 substrates (before sorting for extracellular proteins), predominantly showed chymotryptic-like cleavage specificity of KLK7 by cleaving after tyrosine (Y), phenylalanine (F), leucine (L) and methionine (M) at the P1 position, where the scissile peptide bond is located. Chymotryptic-like cleavages of KLK7 and tryptic-like cleavage specificities cleaving c-terminal to arginine/R were observed in accordance with the KLK7 cleavage site specificity profile obtained in other studies (15, 36, 39, 40). Additionally, non-chymotryptic-like cleavage site specificities, such as serine (S), proline (P), glutamine (E), alanine (A), glycine (G), threonine (T), isoleucine (I), valine (V), glutamine (Q) and aspartic acid (D) were observed, which could be proteolytic effects of other proteases activated by KLK7-mediated hydrolysis in cell CM.

Potential KLK7 Role in the Greater Proteolytic Web—The TAILS analysis identified non-KLK7 cleavage preferences at the P1 position, which has not been detected in the literature (36). Thus, these non-KLK7 cleavage preferences were thought to have originated from indirect cleavages that occurred upon KLK7-mediated proteolytic activation of other zymogens or cleavage of inhibitors of other proteases. In view of this, we utilized the TopFINDer web tool to determine potential protease cascades activated by KLK7 (supplemental Table S13, supplemental Table S6). TopFINDer predicted potential KLK7-activated protease cascades involving eleven of the novel substrates, including insulin-like growth factor binding protein 3 (IGFBP3), IGFBP6, ezrin (EZRI), matrix-metalloprotease 2 (MMP2), osteopontin (SPP1), cystatin C (CST3), proprotein convertase subtilisin/kexin type 5 (PCSK5), colla-

with their respective Light/Heavy ratio, count and Log2 value. *D*, Silver-stained 12% SDS-PAGE showing hydrolysis of recombinant (r) pro-MMP10 (400 ng) by recombinant active KLK7 (1/10 −1/1000 molar ratio to rpro-MMP10); buffer and dmKLK7 treatments were used as controls. Arrow heads in colors depict, open: pro-MMP10 full length protein; red: 45 kDa cleavage fragment; yellow: cleavage fragment ~22 and 30 kDa; black: KLK7 or dmKLK7. *E*, Pro-MMP10 treated with KLK7 (black squares) showed increasing fluorescence emission over time compared with the controls. Pro-MMP10 (yellowish brown circles) showed a slight increase in fluorescence emission with the fluorogenic peptide substrate over time, indicating partial activity, because of residual active MMP10 in the recombinant pro-MMP10 protein purchased. KLK7 (red diamonds) or dmKLK7 (green circles) did not show activity with the MMP10 fluorogenic peptide substrate, confirming that fluorescence intensity increases in the KLK-treated pro-MMP10 is because of putative KLK7-activated-pro-MMP10, but not because of residual KLK7 activity. *F*, Bar graph represents end point (at 35 min) of the reactions performed with triplicate biological replicates ($n = 3$) with the error bar representing the standard error of the mean. In all instances blank corrected fluorescence values were plotted.

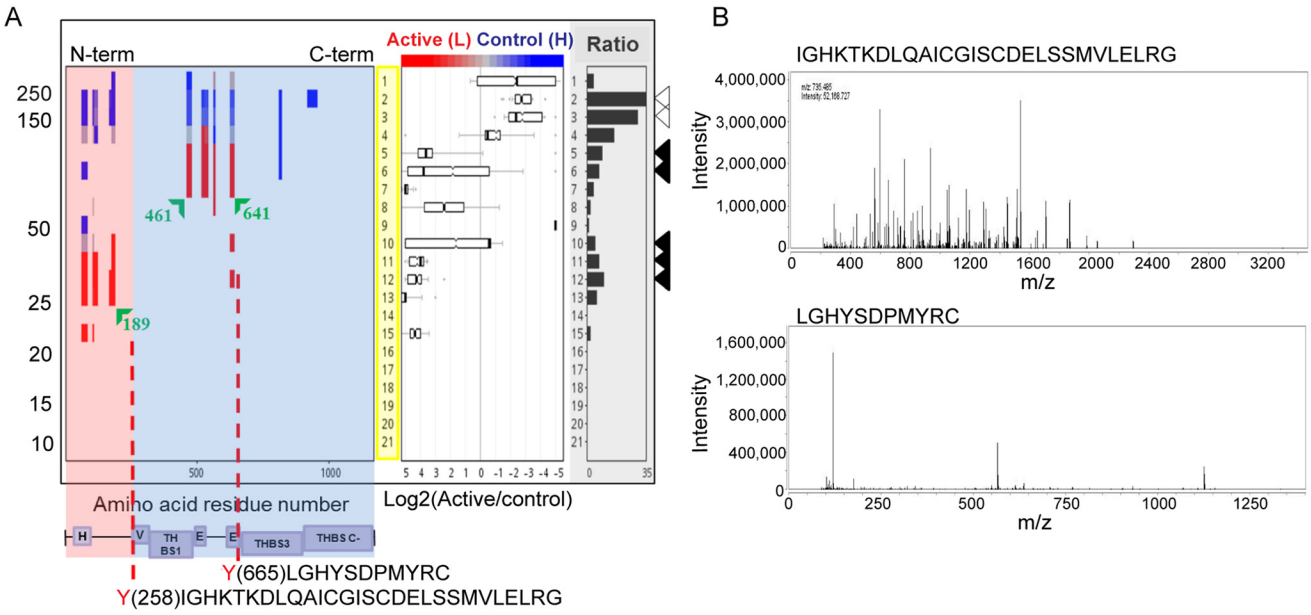

C

Peptide	Position	PEP	Score	PSMs
IEDANLIPPVPDDKFQDLVDAVR	61-83	3.2545E-67	165.38	84
GTLLALER	102-109	5.7701E-13	171.75	28
GTLLALERK	102-110	0.0027752	70.552	1
KDHSGQVFSVVSNGK	110-124	4.0154E-18	125.73	28
DHSGQVFSVVSNGK	165-189	4.2326E-31	153.26	30
AQLYIDCEKMENAELDVPIQSVFTR	174-189	2.8674E-15	95.523	29
MENAELDVPIQSVFTR	461-479	1.4637E-36	146.86	66
LCNSPSPQMNGKPCEGEAR	518-543	9.9966E-65	169.49	98
LCNNPTPQFGGKDCVGDVTENQICNK	530-543	4.0828E-86	178.76	28
DCVGDVTENQICNK	562-571	3.1337E-14	225.79	21
CTSYPDGSWK	624-641	1.2835E-10	144.77	27
FTGSQPFGQGVEHATANK	811-822	1.3917E-96	194.53	73
DNCQYVYNVDQR	920-958	4.1816E-27	164.56	31
DSDGDGRGDACKDDFDHDSVPDIDDICPENVDISETDFR	1078-1091	2.2088E-26	84.369	3

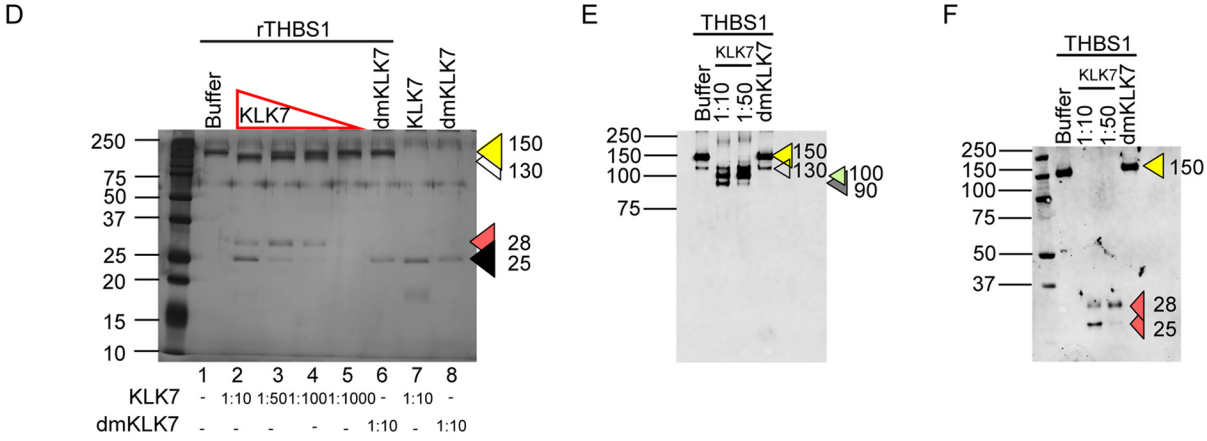

gen, type VII, alpha 1 (COL7A1), midkine (MDK) and annexin-1 (ANXA1) (Fig. 4*B*). Interestingly, substrates that are directly cleaved by KLK7, such as IGFBP3, IGFBP6, MMP2 and MDK, as shown in this as well as other studies are also suggested to be cleaved by indirect pathways. Perhaps in a complex *in vivo* microenvironment both direct and indirect pathways are plausible, and study of these cascades provides the opportunity to understand potential relationships between identified or established KLK7 substrates and putative protein/protease intermediates in the *in vivo* microenvironment.

DISCUSSION

The present study combined two in-depth quantitative proteomics approaches for profiling of the putative substrate repertoire of the KLK7 peptidase *in vitro* as an initial screening for potential physiological targets. Considering that KLK7 is a secreted protease that is activated in the extracellular microenvironment, and the role of the ascites in metastatic ovarian cancer, we used conditioned media (CM) from two ascites-derived cell lines, SKOV-3 and OVMZ-6, to identify the KLK7 degradome and exact cleavage sites using qPROTOMAP and/or TAILS analysis, respectively. We identified 16 novel substrates and two known substrates with high confidence in the secretome of the SKOV-3 cell line using both approaches. On TAILS analysis of the OVMZ-6 secretome, eight substrates were among the 16 SKOV-3 substrates noted above with a further seven OVMZ-6 substrates also identified by the qPROTOMAP approach in SKOV-3 cells. A further 83 putative substrates were identified overall although these still require more comprehensive verification. This is the first study to conduct a comprehensive analysis of the KLK7 degradome in ovarian cancer cell secretomes to define the putative substrate repertoire of KLK7 in this microenvironment.

qPROTOMAP and TAILS approaches, although allows for global substrate identification, are linked with technical bias. For instance, the most abundant proteins are favored, and some proteins were not detected because of peptide loss causing false negative identifications (41, 42). In TAILS it is necessary to perform a LC-MS/MS analysis with pre-TAILS samples (prior to negative selection), to ascertain protein identifications (22). In this study, TAILS protein identifications were limited to those identified in the qPROTOMAP analysis, where protein identifications were made with the protein fragments detected in each gel slice across all replicates spanning the length of the protein. Moreover, in the qPROTOMAP analysis we have used a 1:50 KLK7 to CM (*w*/*w*), whereas a 1:200 (*w*/*w*) ratio was used in the TAILS analysis, potentially leading to identification of a lesser number of cleavage events in the TAILS experiment than in the qPROTOMAP approach.

A large percentage of the proteins identified were of intracellular origin, which may have been released upon cell lysis. In fact, the cancer cell secretome has been shown to consist of classical intracellular proteins released through unconventional pathways (43). Further, intracellular proteins may get secreted into the extracellular microenvironment through vesicles, such as exosomes (43). Although such intracellular proteins secreted into the extracellular microenvironment may still function as signaling molecules that regulate cell-cell communication, only the substrates with an extracellular origin were considered in this study.

In addition to the known KLK7 substrate, MMP2, we have now shown that KLK7 activates MMP10, which in turn, and like that of KLK7, can cleave ECM and basement membrane components (44). Thus, proteolytic processing of these proteins by MMP10 suggests both KLK7-mediated direct and indirect functional effects in cell shedding and cell adhesion to the peritoneal wall initiating metastasis (45). Interestingly, in the KLK7 TAILS analysis COL12A1, a MMP10 substrate, was also cleaved after D^{1139}NTVVLEELRA. This may suggest a potential MMP10-mediated cleavage of COL12A1, because MMP10 cleaves C-terminal to aspartic acid (D) (46).

MMP1, a known cancer promoting peptidase (56) was also identified to be cleaved by KLK7 in the complex secretome microenvironment but not in the biochemical assay (supplemental Fig. S4), suggesting a KLK7-mediated proteolytic event induced by other factors available in cell CM but not in the biochemical assay. Perhaps pro-MMP1 is cleaved

FIG. 2. **KLK7-mediated cleavage of thrombospondin 1.** *A*, Peptograph (replicate 1) representing KLK7-mediated hydrolysis of THBS1 in SKOV-3 cell CM See supplemental Fig. S2 for peptograph description. Arrowheads to the right indicate the migration of THBS1 retrieved from the control (open) and KLK7-generated fragments of THBS1 (filled). The higher molecular weight (MW) peptides (blue and gray) are abundant in gel slices 1–4 (Log2 KLK7/control = 0 to −5), representing the fragments derived from the full-length protein identified in both KLK7- and buffer-treated samples. The lower MW fragments are abundant in gel slices 5–15 (Log2 KLK7/control = 0–5), representing the KLK7 cleavage fragments (red) found in the KLK7-treated sample. A schematic of selected protein domains, based on annotation in the UniProtKB, is shown beneath the X-axis (purple boxes), aligned with the appropriate residues. H, heparin-binding; V, von Willebrand factor, type-C; THBS1/3, THBS type-1/3 repeat; E, epidermal growth factor-like; THBS C-, THBS C-terminal. The TAILS identified KLK7 cleavage sites C-terminal to Y^{258} and Y^{665} are shown by red dotted vertical lines and *B*, represents the respective spectrums. *C*, Peptides identified in the qPROTOMAP analysis (PEP, posterior error probability; Score, The sum of the ion scores of all peptides identified; PSMs, peptide spectrum matches). *D*, Silver-stained 12% SDS-PAGE showing hydrolysis of recombinant (r) THBS1 (500 ng) by recombinant active KLK7 (1/10 −1/1000 molar ratio to rTHBS1); buffer and dmKLK7 treatments were used as controls. Arrow heads in colors depict, yellow: THBS1 full length protein; white: cleavage fragment ~130 kDa; red: 28 kDa cleavage fragment; black: KLK7 or dmKLK7. Western blot analysis of KLK7-treated rTHBS1 using antibodies targeting *E*, full length and *F*, N-terminal THBS1 confirmed the KLK7-mediated generation of N-terminal heparin binding domain containing fragment. Arrowheads indicate different protein products: yellow: full length THBS1, 150 kDa; white: 130 kDa; green: 100 kDa; gray: 90 kDa; red: 28 and 25 kDa fragments. The MW of the protein standard (kDa) is indicated to the left.

TABLE IV
Thirty-seven putative extracellular KLK7 substrates identified in the TAILS analysis of OVMZ-6 cell conditioned media

Accession	Symbol	Protein Description	P1	Peptides	*m/z*	Precursor charge	Probability
Peptidases and peptidase regulators							
#P01034	CST3	cystatin C	125	F.QIYAVPWQGTMTLSKSTCQD.A	1227.1276	2	0.9996
			128	Y.AVPWQGTMTLSKSTCQD.A	1025.0246	2	1
¥Q92743	HTRA1	HtrA serine peptidase 1	286	F.SLQNTVTTGIVSTTQR.G	870.4891	2	1
P06744	GPI	glucose-6-phosphate isomerase	426	L.ANFLAQTEALMR.G	699.8846	2	0.9971
Q9Y287	ITM2B	integral membrane protein 2B	254	F.ENKFAVETLIC.S	739.9136	2	0.9999
P10646	TFPI	tissue factor pathway inhibitor	247	Y.SGCGGNENNFTSKQECLR.A	1063.5051	2	1
			209	F.EFHGPSWCLTPADR.G	853.9121	2	1
Pathway inhibitors							
#Q9UBP4	DKK3	dickkopf WNT signaling pathway inhibitor 3	128	F.SETVITSVGDEEGRR.S	834.9341	2	0.9998
ECM/basement membrane constituents and ECM/ growth factor regulators							
¥Q14512	FGFBP1	fibroblast growth factor binding protein 1	97	A.GNPTSCLKLKDER.V	810.4851	2	0.9996
P51858	HDGF	hepatoma-derived growth factor	79	R.KGFSEGLWEIENNPTVKASGY.Q	810.1128	3	0.9991
#P24592	IGFBP6	insulin like growth factor binding protein 6	219	G.KSLPGSPDGNGSSSCPTGSS.G	1002.4841	2	0.9999
			218	M.GKSLPGSPDGNGSSSCPTGSS.G	1030.9951	2	1
			179	Y.RGAQTLYVPNCDHR.G	860.9416	2	0.9365
*P21741	MDK	midkine (neurite growth-promoting factor 2)	88	F.ENWGACDGGTGTKVR.Q	838.4281	2	1
			87	K.FENWGACDGGTGTKVR.Q	911.9626	2	1
			29	K.KGGPGSECAEWAWGPCTPSSKDCGVGFR.E	1048.1725	3	0.9963
			86	Y.KFENWGACDGGTGTKVR.Q	993.0416	2	1
#P09486	SPARC	secreted protein, acidic, cysteine-rich (osteonectin)	179	Y.ERDEDNNLLTEKQKLR.V	1052.1161	2	0.9983
Cell adhesion molecules/regulators and signal transducers/cell surface receptors							
¥P05067	APP	amyloid beta precursor protein	433	Q.HFQEKVESLEQEAANER.Q	1056.5531	2	1
P63092	GNAS	GNAS complex locus	318	Y.TTPEDATPEPGEDPR.V	823.3916	2	1
Q13421	MSLN	mesothelin	67	L.GFPCAEVSGLSTER.V	772.3851	2	0.9957
O95631	NTN1	netrin 1	251	F.SRLHTFGDENEDDSELAR.D	1063.0036	2	0.9983
			254	L.HTFGDENEDDSELAR.D	884.8951	2	1
Q99985	SEMA3C	semaphorin 3C	499	Y.VSSNEGVSQVSLHR.C	766.9156	2	1
Q08629	SPOCK1	sparc/osteonectin, cwcv and kazal-like domains proteoglycan (testican) 1	22	R.HLDALAGGAGPNHGN.F	717.8686	2	1
Q9UDY2	TJP2	tight junction protein 2	459	F.KSTGDIAGTVVPETNKEPR.Y	1051.1211	2	0.9998
Cytoskeletal proteins/regulators							
¥P61160	ACTR2	ARP2 actin-related protein 2 homolog (yeast)	356	L.GGAVLADIMKDKDNFWMTR.Q	1135.6296	2	1
#P15311	EZR	ezrin	547	R.THNDIIHNENMR.Q	764.3811	2	0.9998
			579	R.IDEFEA.L	764.3811	2	0.9998
			295	R.KPDTIEVQQM.K	628.8631	2	0.9973
O75781	PALM	paralemmin	56	L.EGTPSSASEGDEDLRR.Q	870.4161	2	1
¥Q9Y490	TLN1	talin 1	1575	F.ASNPEFSSIPAQISPEGR.A	960.9971	2	1
Other (Ion channel, galactoside/carbohydrate/ lipid binding and transporters							
#P61769	B2M	beta-2-microglobulin	85	L.YYTEFTPTEKDEYACR.V	1071.0121	2	0.9999
			87	Y.TEFTPTEKDEYACR.V	907.9486	2	1
			86	Y.YTEFTPTEKDEYACR.V	989.4806	2	1
			108	S.QPKIVKWDRD.M	759.4716	2	0.9996

TABLE IV—*continued*

Accession	Symbol	Protein Description	P1	Peptides	*m/z*	Precursor charge	Probability
P54105	CLNS1A	chloride channel, nucleotide-sensitive, 1A	168	Y.TYEEGLSHLTAEGQATLER.L	1070.0426	2	0.9998
#O94985	CLSTN1	calsyntenin 1	169	Y.KATVIEGKQYDSILR.V	912.0781	2	1
Q6UVK1	CSPG4	chondroitin sulfate proteoglycan 4	1856	L.SVVDPDSAPGEIEYEVQR.A	1012.5051	2	1
P17931	LGALS3	lectin, galactoside-binding, soluble, 3	107	Y.GAPAGPLIVPYNLPLPGGVVPR.M	1094.6566	2	1
#Q08380	LGALS3BP	lectin, galactoside-binding, soluble, 3 binding protein	442	Y.SSDYFQAPSDYR.Y	735.3416	2	0.9997
P29122	PCSK6	proprotein convertase subtilisin/kexin type 6	302	Y.SASWGPDDDGKTVDGPGR.L	942.9716	2	1
¥Q8NBP7	PCSK9	proprotein convertase subtilisin/kexin type 9	418	F.SAKDVINEAWFPEDQR.V	987.0236	2	1
			400	L.SAEPELTLAELR.Q	681.8881	2	0.9976
			183	Y.LLDTSIQSDHREIEGR.V	952.0081	2	0.9919
#P07602	PSAP	prosaposin	171	F.MANIPLLLYPQDGPR.S	866.4871	2	0.9995
			172	M.ANIPLLLYPQDGPR.S	800.9671	2	1
O95810	SDPR	serum deprivation response	395	Y.EGSYALTSEEAER.S	738.3571	2	0.9998
Q9ULF5	SLC39A10	solute carrier family 39 (zinc transporter), member 10	80	F.GLEKLLTNLGLGER.K	791.0041	2	1
O14745	SLC9A3R1	solute carrier family 9, subfamily A (NHE3, cation proton antiporter 3), member 3 regulator 1	180	R.SVDPDSPAEASGLR.A	717.8676	2	0.9942
Oxidative stress-related							
O43827	ANGPTL7	angiopoietin like 7	271	F.STKDKDNDNCLDKCAQLR.K	773.0898	3	0.9987
Inflammatory response							
¥P04083	ANXA1	annexin A1	56	M.VKGVDEATIIDILTKR.N	625.0787	3	0.9983
O95407	TNFRSF6B	tumor necrosis factor receptor superfamily member 6b	233	L.QALEAPEGWGPTPR.A	771.9096	2	0.9891
			261	L.TELLGAQDGALLVR.L	745.4436	2	0.9998
			90	Y.CNVLCGEREEEAR.A	828.3881	2	0.944

Accession, reviewed UniProt KB accession; Symbol, UniProtKB/Swiss-Prot entry name prefix (all _HUMAN) with HUGO gene name for UniProtKB entries; Protein Description, UniProtKB protein description; P1, KLK7 cleaves C-terminal to; Peptides, TAILS-identified peptides with "." indicating respective semi-tryptic cleavage sites; *Established KLK7 substrate; #Substrates identified in both SKOV-3 and OVMZ-6 cell CM by TAILS analysis; ¥Substrates identified in qPROTOMAP and TAILS analysis of SKOV-3 and OVMZ-6 cell CM respectively.

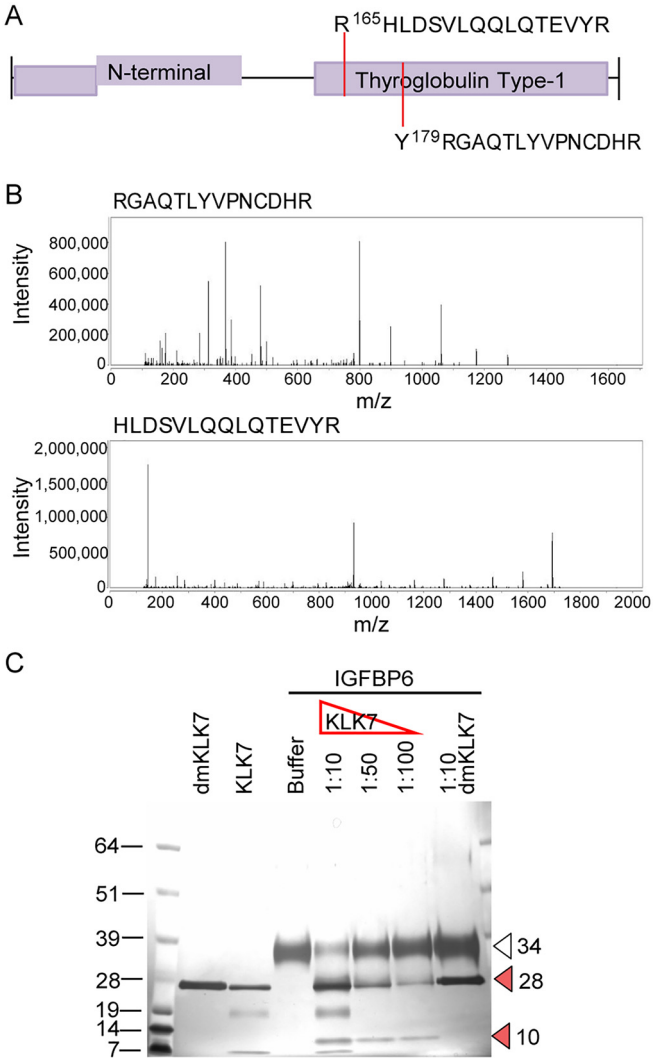

FIG. 3. **KLK7-mediated hydrolysis of IGFBP6 in SKOV-3 and OVMZ-6 cell CM.** *A*, TAILS-identified cleavage sites are indicated by dotted lines on the schematic of selected protein domains, based on annotation in the UniProtKB. *B*, Respective spectra of the TAILS-identified peptides. *C*, Silver-stained 12% SDS-PAGE showing hydrolysis of recombinant IGFBP6. Arrowheads indicate: open: full length IGFBP6, 34 kDa; red: cleaved IGFBP6 fragments, 10 and 28 kDa. The molecular weight (MW) of the protein standard (kDa) is indicated to the left.

by another protease activated by KLK7-mediated proteolytic activity or another factor may have stimulated the KLK7-mediated cleavage of pro-MMP1 in the complex pool of proteins secreted by SKOV-3 cells. The cleavage sites identified for MMP1 in the TAILS assay have chymotryptic-like cleavage site preferences, suggesting a KLK7-mediated activation of another chymotryptic-like protease in the SKOV-3 cell CM. This observation implies the potential of KLK7-activated protease cascades and the bias associated with the use of biochemical assays to determine peptidase substrates emphasizing the importance of proteomics analysis of complex protein pools, as in the present study, to determine putative substrates of peptidases that are aberrantly expressed in cancer. However, any functional effect of this KLK7-mediated cleavage of MMP1 is not clear and requires further functional validation. Nonetheless, these combined findings on KLK7 cleavage of several MMPs point to a potentially critical proteolytic interaction in the ovarian tumor microenvironment.

The current study reported a KLK7-mediated cleavage of THBS1, producing a 28 kDa N-terminal fragment, using both the qPROTOMAP and TAILS approaches. Cleavage of THBS1 N terminus has been already reported in the literature, where A disintegrin and metalloproteinase with thrombospondin motifs (ADAMTS)-1 (47), thrombin (48), and cathepsin G (49) were shown to cleave THBS1, generating similar N-terminal THBS1 fragments, of 36 kDa, 25 kDa, and 28 kDa, respectively. Interestingly, the N-terminal 28 kDa fragment was previously shown to promote angiogenesis through a syndecan-4 proteoglycan-dependent pathway (50), although full length THBS1 actively inhibits angiogenesis by inducing receptor-mediated apoptosis in activated endothelial cells (51). Further, high levels of THBS1 in high grade ovarian cancer patients are associated with improved survival because of inhibition of angiogenesis (52).

Insulin-like growth factor binding protein (IGFBP) 6 was proteolytically processed in both SKOV-3 and OVMZ-6 cell CM. IGFBP6 has been shown to promote cell migration (53), suppress cellular proliferation (54) and inhibit angiogenesis (55) in other cancers, suggesting a cancer promoting as well as a suppressive role, but has not been widely studied in the ovarian cancer context. However, IGFBP6 have been shown to be lowly expressed in ovarian cancer patients compared with the healthy controls (56). TAILS-determined cleavage of IGFBP6 suggests a cleavage in the thyroglobulin type-1 domain, the consequences of which is yet to be interrogated.

We observed a significant difference in the pool of cell secreted proteins by the two cell lines employed. Importantly, the OVMZ-6 line is from a FIGO Stage IV poorly differentiated serous adenocarcinoma (14) whereas the SKOV-3 cell line is derived from a patient with moderately well differentiated adenocarcinoma (12, 13) so heterogeneity of cell secreted proteins would be expected (57). Despite the heterogeneity of cell secreted proteins, the GO-annotated biological functions suggested that KLK7-mediated proteolytic processing of these different substrates ultimately led to classical KLK7 functions that had been identified to date, such as cell shedding and ECM remodeling. Notably, we still identified 15 common KLK7 substrates in the secretome of these 2 cell lines.

In accordance with the KLK7 cleavage site specificity profile obtained in other studies, KLK7-derived peptides showed primarily chymotryptic- (Y, F, L and M) and tryptic-like (R) cleavage site specificities (36, 39, 40). This is the first study to determine KLK7 cleavage site specificities using human-derived full-length proteins as the library and thus determin-

TABLE V
Peptides identified in MS analysis of KLK7-generated IGFBP6 fragment

	Sequence	Modifications	# PSMs	# Missed Cleavages	Theo. MH+ [Da]	Abundances (Grouped): Sample	XCorr	Top Apex RT [min]
A182	QTLYVPNCDHR	1×Carbamidomethyl [C8]; 1×Dimethyl [N-Term]	1	0	1430.685		2.88	
G81	LQCHPPKDDEAPLR	1×Carbamidomethyl [C3]; 1×Dimethyl [K7]; 1×Dimethyl [N-Term]	1	1	1731.885		3.78	
Q156	DTEMGPCR	1×Carbamidomethyl [C7]; 1×Dimethyl [N-Term]	1	0	993.4128		2.34	
N151	SAGVQDTEMGPCR	1×Carbamidomethyl [C12]; 1×Oxidation [M9]; 1×Dimethyl [N-Term]	1	0	1451.625		4.2	
A27	RCPGCGQGVQAGCPGGCVEEEDGGSPAEGCAEAEGCLRR	6×Carbamidomethyl [C2; C5; C13; C17; C30; C36]; 1×Dimethyl [N-Term]	15	2	4164.71	1.00E+09	9.79	15.16
*Y179	RGAQTLYVPNCDHR	1×Carbamidomethyl [C11]; 1×Dimethyl [N-Term]	3	1	1714.844	3.00E+08	4.32	14.05
Y74	TPNCAPGLQCHPPKDDEAPLR	2×Carbamidomethyl [C4; C10]; 1×Dimethyl [K14]; 1×Dimethyl [N-Term]	3	1	2429.17	2.00E+08	6.1	14.8
A27	RCPGCGQGVQAGCPGGCVEEEDGGSPAEGCAEAEGCLR	6×Carbamidomethyl [C2; C5; C13; C17; C30; C36]; 1×Dimethyl [N-Term]	10	1	4008.609	2.00E+08	9.75	15.54
L185	YVPNCDHR	1×Carbamidomethyl [C5]; 1×Dimethyl [N-Term]	3	0	1088.494	9.00E+07	2.65	11.1
N51	SAGVQDTEMGPCRR	1×Carbamidomethyl [C12]; 1×Dimethyl [N-Term]	2	1	1591.732	7.00E+07	4.38	13.95
N151	SAGVQDTEMGPCRR	1×Carbamidomethyl [C12]; 1×Oxidation [M9]; 1×Dimethyl [N-Term]	2	1	1607.726	5.00E+07	3.42	13.62
Q37	AGCPGGCVEEEDGGSPAEGCAEAEGCLRR	4×Carbamidomethyl [C3; C7; C20; C26]; 1×Dimethyl [N-Term]	2	1	3065.245	5.00E+07	5.58	15.26
N77	CAPGLQCHPPKDDEAPLR	2×Carbamidomethyl [C1; C7]; 1×Dimethyl [K11]; 1×Dimethyl [N-Term]	3	1	2117.027	2.00E+07	6.33	14.69
N151	SAGVQDTEMGPCR	1×Carbamidomethyl [C12]; 1×Dimethyl [N-Term]	1	0	1435.63	2.00E+07	3.9	14.62
A38	GCPGGCVEEEDGGSPAEGCAEAEGCLRR	4×Carbamidomethyl [C2; C6; C19; C25]; 1×Dimethyl [N-Term]	3	1	2994.208	9.00E+06	5.14	15.24
Q37	AGCPGGCVEEEDGGSPAEGCAEAEGCLR	4×Carbamidomethyl [C3; C7; C20; C26]; 1×Dimethyl [N-Term]	1	0	2909.144	7.00E+06	7.56	15.84
*R165	HLDSVLQQL	1×Dimethyl [N-Term]	1	0	1080.605	5.00E+06	2.09	18.92
A111	VAEENPKESKPQAGTARPQDVNRR	2×Dimethyl [K7; K10]; 1×Dimethyl [N-Term]	1	2	2761.47	5.00E+06	4.75	13.6
R209	GPCWCVDR	2×Carbamidomethyl [C3; C5]; 1×Dimethyl [N-Term]	1	0	1077.46	4.00E+06	2.16	15.55
G51	SPAEGCAEAEGCLRR	2×Carbamidomethyl [C6; C12]; 1×Dimethyl [N-Term]	1	1	1690.764	2.00E+06	2.81	14.13
R208	RGPCWCVDR	2×Carbamidomethyl [C4; C6]; 1×Dimethyl [N-Term]	1	1	1233.562	2.00E+06	2.94	14.43
Q34	GVQDTEMGPCRR	1×Carbamidomethyl [C10]; 1×Dimethyl [N-Term]	1	1	1433.662	2.00E+06	3.2	13.83
G142	TSTTPSQPNSAGVQDTEMGPCRR	1×Carbamidomethyl [C21]; 1×Dimethyl [N-Term]	1	1	2505.146	2.00E+06	4.3	14.57
A38	GCPGGCVEEEDGGSPAEGCAEAEGCLR	4×Carbamidomethyl [C2; C6; C19; C25]; 1×Dimethyl [N-Term]	1	0	2838.107	1.00E+06	5.81	15.81
R180	GAQTLYVPNCDHR	1×Carbamidomethyl [C10]; 1×Dimethyl [N-Term]	1	0	1558.743	9.00E+05	3.6	14.8
G51	SPAEGCAEAEGCLR	2×Carbamidomethyl [C6; C12]; 1×Dimethyl [N-Term]	1	0	1534.662	5.00E+05	2.02	14.61
Q183	TLYVPNCDHR	1×Carbamidomethyl [C7]; 1×Dimethyl [N-Term]	1	0	1302.626	4.00E+05	2.57	14.84

PSMs, peptide spectrum matches; Theo MH+, protonated monoisotopic mass of the peptides in Daltons; XCorr, A search-dependent score - it scores the number of fragment ions that are common to two different peptides with the same precursor mass and calculates the cross-correlation score for all candidate peptides queried from the database by SEQUEST searches; RT (min), the peptide's retention time during chromatographic separation; and *peptides identified in TAILS analysis. Peptides are sorted according to the "Abundances (grouped samples)" column.

TABLE VI
Gene Ontology-annotated biological processes for TAILS-identified putative extracellular KLK7 substrates in SKOV-3 and OVMZ-6 cell conditioned media

GOTERM_BP_FAT	*P* Value	Symbol
SKOV-3		
GO:0007155~cell adhesion	4.31E-06	COL7A1, EZR, NID2, CDH6, COL12A1, LGALS3BP, THBS1, CLSTN1
GO:0022610~biological adhesion	4.35E-06	COL7A1, EZR, NID2, CDH6, COL12A1, LGALS3BP, THBS1, CLSTN1
GO:0030574~collagen catabolic process	2.16E-04	MMP2, MMP10, MMP1
GO:0044243~multicellular organismal catabolic process	3.67E-04	MMP2, MMP10, MMP1
GO:0032963~collagen metabolic process	4.27E-04	MMP2, MMP10, MMP1
GO:0044259~multicellular organismal macromolecule metabolic process	5.24E-04	MMP2, MMP10, MMP1
GO:0044236~multicellular organismal metabolic process	7.47E-04	MMP2, MMP10, MMP1
GO:0001501~skeletal system development	0.004787827	MMP2, SPARC, COL12A1, FBN1
OVMZ-6		
GO:0006928~cell motion	1.80E-04	ACTR2, ANXA1, TLN1, SEMA3C, NTN1, SPOCK1, APP

GOTERM_BP_FAT, summarized version of biological processes in the Gene Ontology (GO) database; *P* Value, calculated using a modified Fisher Exact test; Symbol, UniProtKB/Swiss-Prot entry name prefix (all _HUMAN) with HUGO gene name for UniProtKB entries

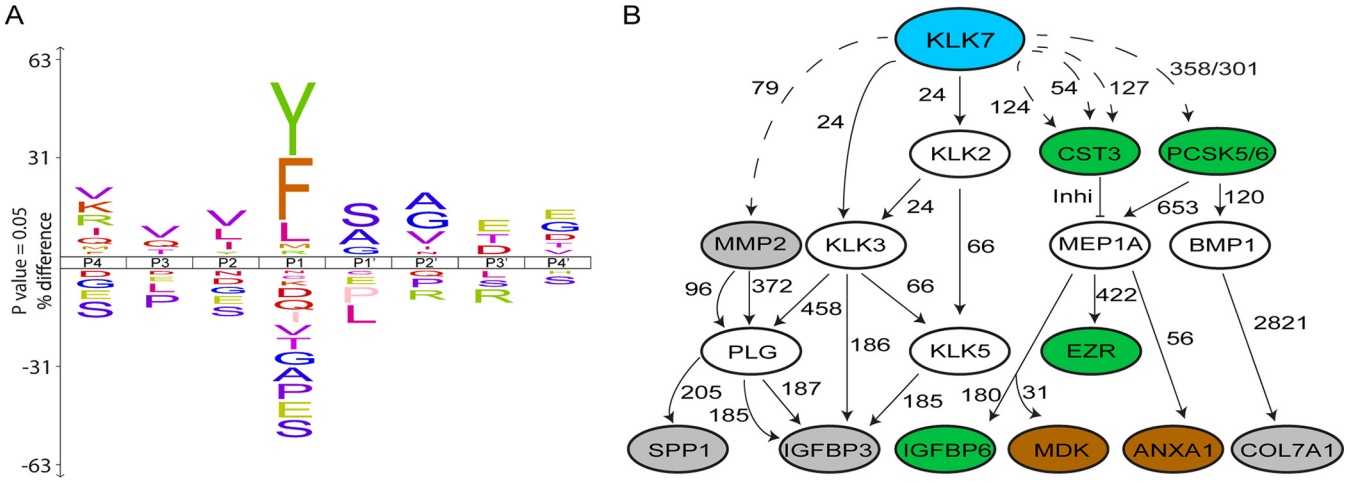

FIG. 4. **KLK7 subsite preferences and potential role in the greater proteolytic web.** *A*, To determine KLK7 subsite preferences, TAILS-identified cleavage sites are displayed as IceLogos representation by comparing both the positive and negative frequency percentage of an amino acid (vertical axis) at a certain location in the multiple sequence alignment (horizontal axis) and the Swiss-Prot *Homo sapiens* protein database. KLK7 showed chymotryptic-like specificities by cleaving C-terminal to tyrosine (Y), phenylalanine (F) and leucine (L). The height of the single amino acid residue reflects its occurrence rate for each position in P4-P4′. Amino acid residues are color coded according to their physico-chemical properties. Sequence logo *x* axis indicates percent difference at a *p* value of 0.05%. *B*, Potential association of KLK7 with TAILS-identified (11) substrates, determined using the TopFINDer (v3.0) software. Blue oval, protease of interest, KLK7; gray ovals, TAILS-identified KLK7 substrates in SKOV-3 cell line; brown ovals, TAILS-identified KLK7 substrates in OVMZ-6 cell line; green ovals, TAILS-identified substrates in both cell lines; open ovals, KLK7 substrates known to date and putative intermediate proteins; dotted line, cleavages identified in TAILS; solid lines, recorded cleavage events in MEROPS; and numbers, amino acid residues at cleavage sites.

ing the physiological cleavage specificities of KLK7. In this analysis, specificities other than chymotryptic- and tryptic-like cleavages were also observed, which could have originated from indirect cleavage events from proteases activated by KLK7-mediated proteolytic processing, such as MMP10.

The present study has contributed greatly to the knowledge of the KLK7 degradome in the ovarian cancer microenvironment by increasing the existing list of KLK7 substrates. The novel putative extracellular KLK7 substrates identified in the secretome of two distinct ovarian cancer ascites-derived cell lines using two proteomics approaches will help determine the physiological substrates of KLK7 and mechanisms underlying the functional roles of KLK7. Further, it provides a large data source of 83 putative substrates, which can be interrogated for future studies analyzing the mechanistic and functional role of KLK7 in this cancer and may be extrapolated to other cancers as well.

Similar studies should also be conducted on other KLKs and other proteases, which may help in delineating the role of these peptidases in the greater proteolytic web.

DATA AVAILABILITY

MS data have been deposited to the ProteomeXchange consortium (http://proteomecentral.proteomexchange.org) via the PRIDE partner repository. Zipped MaxQuant ".txt" files including ".wiff" files have been deposited with the dataset identifier PXD003812 for SKOV-3 qPROTOMAP analysis. The TAILS MS files have been deposited with the dataset identifier PXD003752 or DOI: 10.6019/PXD003752 for SKOV-3 and PXD004591 or DOI: 10.6019/PXD004591 for OVMZ-6.

* This work was funded by grants-in-aid from the National Health and Medical Research Council of Australia (553045), Australia-India Strategic Research Fund (BF060023), the Cancer Council Queensland (1051318, 1105922), Wesley Research Institute Foundation (2010-07) and the DAAD Deutsch-Australisches Netzwerk der Personalisierten Krebsmedizin. Access to proteomic infrastructure in the QIMR Berghofer Protein Discovery Centre was made possible by funding from Bioplatforms Australia and the Queensland State Government provided through the Australian Government National Collaborative Infrastructure Strategy (NCRIS) and EIF Fund. JAC is a Principal Research Fellow of the National Health and Medical Research Council of Australia (1005717).

[S] This article contains supplemental Figures and Tables.

‡‡ To whom correspondence may be addressed: National Institute of Dental and Craniofacial Research, 30 Convent Drive, Bethesda, MD 20892. Tel.: +1 301 435 1841; E-mail: munasinghage.silva@nih.gov.

§§ To whom correspondence may be addressed: Queensland University of Technology (QUT), Institute of Health and Biomedical Innovation (IHBI) and School of Biomedical Sciences at the Translational Research Institute, 37 Kent Street, Woolloongabba, QLD 4102, Australia.: Tel.: +61 734 437 241; +61 407 074 032; Fax: +61 734 437 779; E-mail: j.clements@qut.edu.au.

** Present addresses: National Institute of Dental and Craniofacial Research, 30 Convent Drive, Bethesda, Maryland 20892 (L.M.S.); Mater Research Institute – The University of Queensland, Translational Research Institute, Woolloongabba, Queensland, 4102, Australia (T.K.); The University of Queensland Diamantina Institute at the Translational Research Institute, 37 Kent Street, Woolloongabba, Queensland, 4102, Australia (C.R.S.); Faculty of Biology, Technion Israel institute of Technology, Haifa, 32000 Israel (O.K.).

Author contributions: J.A.C., L.M.S., and Y.D. designed research; L.M.S., T.K., T.S., and M.L.H. performed research; C.R.S. produced constructs for KLK7 production; O.K., and J.J.G. contributed reagents and/or mass spectrometry facilities; V.M. provided cell lines and constructive advice; J.J.G. provided strategic guidance during this project; L.M.S., T.S., and C.H. analyzed data; L.M.S. wrote the manuscript; all authors reviewed the manuscript.

REFERENCES

1. Siegel, R. L., Miller, K. D., and Jemal, A. (2016) Cancer statistics, 2016. *CA Cancer J. Clin.* **66,** 7–30
2. Bhoola, S., and Hoskins, W. J. (2006) Diagnosis and Management of Epithelial Ovarian Cancer. *Obstet. Gynecol.,* **107,** 1399–1410
3. Puls, L. E., Duniho, T., Hunter, J. E., Kryscio, R., Blackhurst, D., and Gallion, H. (1996) The prognostic implication of ascites in advanced-stage ovarian cancer. *Gynecol. Oncol.* **61,** 109–112
4. Dong, Y., Tan, O. L., Loessner, D., Stephens, C., Walpole, C., Boyle, G. M., Parsons, P. G., and Clements, J. A. (2010) Kallikrein-related peptidase 7 promotes multicellular aggregation via the $\alpha5\beta1$ integrin pathway and paclitaxel chemoresistance in serous epithelial ovarian carcinoma. *Cancer Res.* **70,** 2624
5. Ahmed, N., and Stenvers, K. L. (2013) Getting to know ovarian cancer ascites: opportunities for targeted therapy-based translational research. *Front. Oncol.* **3,** 256
6. Prezas, P., Arlt, M. J., Viktorov, P., Soosaipillai, A., Holzscheiter, L., Schmitt, M., Talieri, M., Diamandis, E. P., Krüger, A., and Magdolen, V. (2006) Overexpression of the human tissue kallikrein genes KLK4, 5, 6, and 7 increases the malignant phenotype of ovarian cancer cells. *Biol. Chem.* **387,** 807–811
7. Dorn, J., Bronger, H., Kates, R., Slotta-Huspenina, J., Schmalfeldt, B., Kiechle, M., Diamandis, E. P., Soosaipillai, A., Schmitt, M., and Harbeck, N. (2015) OVSCORE - a validated score to identify ovarian cancer patients not suitable for primary surgery. *Oncol. Lett.* **9,** 418–424
8. Dorn, J., Beaufort, N., Schmitt, M., Diamandis, E.P., Goettig, P., and Magdolen, V. (2014) Function and clinical relevance of kallikrein-related peptidases and other serine proteases in gynecological cancers. *Crit. Rev. Clin. Lab. Sci.* **51,** 63–84
9. Fuhrman-Luck, R. A., Silva, M. L., Dong, Y., Irving-Rodgers, H., Stoll, T., Hastie, M. L., Loessner, D., Gorman, J. J., and Clements, J. A. (2014) Proteomic and other analyses to determine the functional consequences of deregulated kallikrein-related peptidase (KLK) expression in prostate and ovarian cancer. *Proteomics Clin. Appl.* **8,** 403–415
10. Dix, M. M., Simon, G. M., and Cravatt, B. F. (2008) Global mapping of the topography and magnitude of proteolytic events in apoptosis. *Cell* **134,** 679–691
11. Kleifeld, O., et al. (2010) Isotopic labeling of terminal amines in complex samples identifies protein N-termini and protease cleavage products. *Nat. Biotechnol.* **28,** 281–288
12. Fogh, J., Fogh, J. M., and Orfeo, T. (1977) One hundred and twenty-seven cultured human tumor cell lines producing tumors in nude mice. *J. Natl. Cancer Inst.* **59,** 221–226
13. Fogh, J., Wright, W. C., and Loveless, J. D. (1977) Absence of HeLa cell contamination in 169 cell lines derived from human tumors. *J. Natl. Cancer Inst.* **58,** 209–214
14. Mobus, V., Gerharz, C. D., Press, U., Moll, R., Beck, T., Mellin, W., Pollow, K., Knapstein, P. G., and Kreienberg, R. (1992) Morphological, immunohistochemical and biochemical characterization of 6 newly established human ovarian carcinoma cell lines. *Int. J. Cancer* **52,** 76–84
15. Silva, L. M., Stoll, T., Kryza, T., Stephens, C. R., Hastie, M. L., Irving-Rodgers, H. F., Dong, Y., Gorman, J. J., and Clements, J. A. (2017) Mass spectrometry-based determination of Kallikrein-related peptidase 7 (KLK7) cleavage preferences and subsite dependency. *Sci. Rep.* **7,** 6789
16. Vizcaino, J. A., Deutsch, E. W., Wang, R., Csordas, A., Reisinger, F., Ríos, D., Dianes, J. A., Sun, Z., Farrah, T., Bandeira, N., Binz, P. A., Xenarios, I., Eisenacher, M., Mayer, G., Gatto, L., Campos, A., Chalkley, R. J., Kraus, H. J., Albar, J. P., Martinez-Bartolomé, S., Apweiler, R., Omenn, G. S., Martens, L., Jones, A. R., and Hermjakob, H. (2014) ProteomeXchange provides globally coordinated proteomics data submission and dissemination. *Nat. Biotechnol.* **32,** 223–226
17. Ong, S. E., Kratchmarova, I., and Mann, M. (2003) Properties of 13C-substituted arginine in stable isotope labeling by amino acids in cell culture (SILAC). *J. Proteome Res.* **2,** 173–181
18. Shevchenko, A., Tomas, H., Havlis, J., Olsen, J. V., and Mann, M. (2006) In-gel digestion for mass spectrometric characterization of proteins and proteomes. *Nat. Protoc.* **1,** 2856–2860
19. Cox, J., and Mann, M. (2008) MaxQuant enables high peptide identification rates, individualized p.p.b.-range mass accuracies and proteome-wide protein quantification. *Nat. Biotechnol.* **26,** 1367–1372
20. Cox, J., Neuhauser, N., Michalski, A., Scheltema, R. A., Olsen, J.V., and Mann, M. (2011) Andromeda: a peptide search engine integrated into the MaxQuant environment. *J. Proteome Res.* **10,** 1794–1805
21. Dix, M. M., Simon, G. M., Wang, C., Okerberg, E., Patricelli, M. P., and Cravatt, B. F. (2012) Functional interplay between caspase cleavage and phosphorylation sculpts the apoptotic proteome. *Cell* **150,** 426–440
22. Kleifeld, O., Doucet, A., Prudova, A., auf dem Keller, U., Gioia, M., Kizhakkedathu, J. N., and Overall, C. M. (2011) Identifying and quantifying

proteolytic events and the natural N terminome by terminal amine isotopic labeling of substrates. *Nat. Protocols* **6,** 1578–1611
23. Kessner, D., Chambers, M., Burkem, R., Agus, D., and Mallick, P. (2008) ProteoWizard: open source software for rapid proteomics tools development. *Bioinformatics* **24,** 2534–2536
24. Craig, R., and Beavis, R. C. (2004) TANDEM: matching proteins with tandem mass spectra. *Bioinformatics* **20,** 1466–1467
25. Pedrioli, P. G. (2010) Trans-proteomic pipeline: a pipeline for proteomic analysis. *Methods Mol. Biol.* **604,** 213–238
26. Magrane, M., and U. Consortium, (2011) *UniProt Knowledgebase: a hub of integrated protein data.* Database (Oxford), **2011,** p. bar009
27. Mellacheruvu, D., Wright, Z., Couzens, A. L., Lambert, J. P., St-Denis, N. A., Li T., Miteva, Y. V., Hauri, S., Sardiu, M. E., Low, T. Y., Halim, V. A., Bagshaw, R. D., Hubner, N. C., Al-Hakim, A., Bouchard, A., Faubert, D., Fermin, D., Dunham, W. H., Goudreault, M., Lin, Z. Y., Badillo, B. G., Pawson, T., Durocher, D., Coulombe, B., Aebersold, R., Superti-Furga, G., Colinge, J., Heck, A. J., Choi, H., Gstaiger, M., Mohammed, S., Cristea, I. M., Bennett, K. L., Washburn, M. P., Raught, B., Ewing, R. M., Gingras, A. C., and Nesvizhskii, A. I. (2013) The CRAPome: a contaminant repository for affinity purification-mass spectrometry data. *Nat. Methods* **10,** 730–736
28. Keller, A., Eng J., Zhang, N., Li, X. J., and Aebersold, R. (2005) A uniform proteomics MS/MS analysis platform utilizing open XML file formats. *Mol. Syst. Biol.* **1,** 0017
29. auf dem Keller, U., Prudova, A., Gioia, M., Butler, G. S., and Overall, C. M. (2010) A statistics-based platform for quantitative N-terminome analysis and identification of protease cleavage products. *Mol. Cell. Proteomics* **9,** 912–927
30. Fortelny, N., Yang, S., Pavlidis, P., Lange, P. F., and Overall, C. M. Proteome TopFIND 3.0 with TopFINDer and PathFINDer: database and analysis tools for the association of protein termini to pre- and post-translational events. *Nucleic Acids Res.* **43,** D290–D297
31. Huang da, W, Sherman, B. T., and Lempicki, R. A. (2009) Systematic and integrative analysis of large gene lists using DAVID bioinformatics resources. *Nat. Protoc.* **4,** 44–57
32. Sondell, B., Dyberg, P., Anneroth, G. K., Ostman, P. O., and Egelrud, T. (1996) Association between expression of stratum corneum chymotryptic enzyme and pathological keratinization in human oral mucosa. *Acta Dermato-venereologica* **76,** 177–181
33. Ramani, V. C., and Haun, R. S. (2008a) The extracellular matrix protein fibronectin is a substrate for kallikrein 7. *Biochem. Biophys. Res. Commun.* **369,** 1169–1173
34. Ramani, V. C., Kaushal, G. P., and Haun, R. S. (2011) Proteolytic action of kallikrein-related peptidase 7 produces unique active matrix metalloproteinase-9 lacking the C-terminal hemopexin domains. *Biochim. Biophys. Acta* **1813,** 1525
35. Yu, Y., Prassas, I., Dimitromanolakis, A., and Diamandis, E.P. (2015) Novel biological substrates of human kallikrein 7 identified through degradomics. *J. Biol. Chem.,* **290,** 17762–17775
36. Skytt, A., Stromqvist, M., and Egelrud, T. (1995) Primary substrate specificity of recombinant human stratum corneum chymotryptic enzyme. *Biochem. Biophys. Res. Commun.* **211,** 586–589
37. Lawrence, M. G., Lai, J., and Clements, J. A. (2010) Kallikreins on steroids: structure, function, and hormonal regulation of prostate-specific antigen and the extended kallikrein locus. *Endocrine reviews,* **31,** 407–446
38. Borgono, C. A., and Diamandis, E. P. (2004) the emerging roles of human tissue kallikreins in cancer. *Nature Rev.* **4,** 876–890
39. Debela, M., Magdolen, V., Schechter, N., Valachova, M., Lottspeich, F., Craik, C. S., Choe, Y., Bode, W., and Goettig, P. (2006) Specificity profiling of seven human tissue kallikreins reveals individual subsite preferences. *J. Biol. Chem.* **281,** 25678–25688
40. Oliveira, J. R., Bertolin, T. C., Andrade, D., Oliveira, L. C., Kondo, M. Y., Santos, J. A., Blaber, M., Juliano, L., Severino, B., Caliendo, G., Santagada, V., and Juliano, M. A. (2015) Specificity studies on Kallikrein-related peptidase 7 (KLK7) and effects of osmolytes and glycosaminoglycans on its peptidase activity. *Biochim. Biophys. Acta* **1854,** 73–83
41. Speicher, K. D., Kolbas, O., Harper, S., and Speicher, D. W. (2000) Systematic analysis of peptide recoveries from in-gel digestions for protein identifications in proteome studies. *J. Biomol. Tech.* **11,** 74–86
42. Rappsilber, J., Mann, M., and Ishihama, Y. (2007) Protocol for micro-purification, enrichment, pre-fractionation and storage of peptides for proteomics using StageTips. *Nat. Protoc.* **2,** 1896–1906
43. Sinha, A., Ignatchenko, V., Ignatchenko, A., Mejia-Guerrero, S., and Kislinger, T. (2014) In-depth proteomic analyses of ovarian cancer cell line exosomes reveals differential enrichment of functional categories compared to the NCI 60 proteome. *Biochem. Biophys. Res. Commun.* **445,** 694–701
44. Schlage, P., Kockmann, T., Kizhakkedathu, J. N., and auf dem Keller, U. (2015) Monitoring matrix metalloproteinase activity at the epidermal-dermal interface by SILAC-iTRAQ-TAILS. *Proteomics* **15,** 2491–2502
45. Justilien, V., Regala, R. P., Tseng, I. C., Walsh, M. P., Batra, J., and Radisky, E. S., Murray, N. R., Fields A. P. (2012) Matrix metalloproteinase-10 is required for lung cancer stem cell maintenance, tumor initiation and metastatic potential. *PLoS ONE* **7,** e35040
46. Schlage, P., Kockmann, T., Kizhakkedathu, J. N., and auf dem Keller, U. (2015) Monitoring matrix metalloproteinase activity at the epidermal-dermal interface by SILAC-iTRAQ-TAILS. *Proteomics* **15,** 2491–2502
47. Lee, N. V., Sato, M., Annis, D. S., Loo, J. A., Wu, L., Mosher, D. F., and Iruela-Arispe, M. L. (2006) ADAMTS1 mediates the release of antiangiogenic polypeptides from TSP1 and 2. *EMBO J.* **25,** 5270–5283
48. Lawler, J., Connolly, J. E., Ferro, P., and Derick, L. H. (1986) Thrombin and chymotrypsin interactions with thrombospondin. *Ann. N.Y. Acad. Sci.* **485,** 273–287
49. Rabhi-Sabile, S., Pidard, D., Lawler, J., Renesto, P., Chignard, M., and Legrand, C. (1996) Proteolysis of thrombospondin during cathepsin-G-induced platelet aggregation: functional role of the 165-kDa carboxy-terminal fragment. *FEBS Lett.* **386,** 82–86
50. Ferrari do Outeiro-Bernstein, M. A., Nunes, S. S., Andrade, A. C., Alves, T. R., Legrand, C., and Morandi, V. (2002) A recombinant NH(2)-terminal heparin-binding domain of the adhesive glycoprotein, thrombospondin-1, promotes endothelial tube formation and cell survival: a possible role for syndecan-4 proteoglycan. *Matrix Biol.* **21,** 311–324
51. Jimenez, B., Volpert, O. V., Crawford, S. E., Febbraio, M., Silverstein, R. L., and Bouck, N. (2000) Signals leading to apoptosis-dependent inhibition of neovascularization by thrombospondin-1. *Nat. Med.* **6,** 41–48
52. Alvarez, A. A., Axelrod, J. R., Whitaker, R. S., Isner, P. D., Bentley, R. C., Dodge, R. K., and Rodriguez, G. C. (2001) Thrombospondin-1 expression in epithelial ovarian carcinoma: association with p53 status, tumor angiogenesis, and survival in platinum-treated patients. *Gynecol. Oncol.* **82,** 273–278
53. Fu, P., Thompson, J. A., and Bach, L. A. (2007) Promotion of cancer cell migration: an insulin-like growth factor (IGF)-independent action of IGF-binding protein-6. *J. Biol. Chem.* **282,** 22298–22306
54. Koike, H., Ito, K., Takezawa, Y., Oyama, T., Yamanaka, H., and Suzuki, K. (2005) Insulin-like growth factor binding protein-6 inhibits prostate cancer cell proliferation: implication for anticancer effect of diethylstilbestrol in hormone refractory prostate cancer. *Br. J. Cancer* **92,** 1538–1544
55. Zhang, C., Lu, L., Li, Y., Wang, X., Zhou, J., Liu, Y., Fu, P., Gallicchio, M. A., Bach, L. A., and Duan, C. (2012) IGF binding protein-6 expression in vascular endothelial cells is induced by hypoxia and plays a negative role in tumor angiogenesis. *Int. J. Cancer* **130,** 2003–2012
56. Gunawardana, C., Kuk, C., Smith, C. R., Batruch, I., Soosaipillai, A., and Diamandis, E. P. (2009) Comprehensive analysis of conditioned media from ovarian cancer cell lines identifies novel candidate markers of epithelial ovarian cancer. *J. Proteome Res.* **8,** 4705–4713
57. Coscia, F., Watters, K. M., Curtis, M., Eckert, M. A., Chiang, C. Y., Tyanova, S., Montag, A., Lastra, R. R., Lengyel, E., and Mann, M. (2016) Integrative proteomic profiling of ovarian cancer cell lines reveals precursor cell associated proteins and functional status. *Nat. Commun.* **7,** 12645